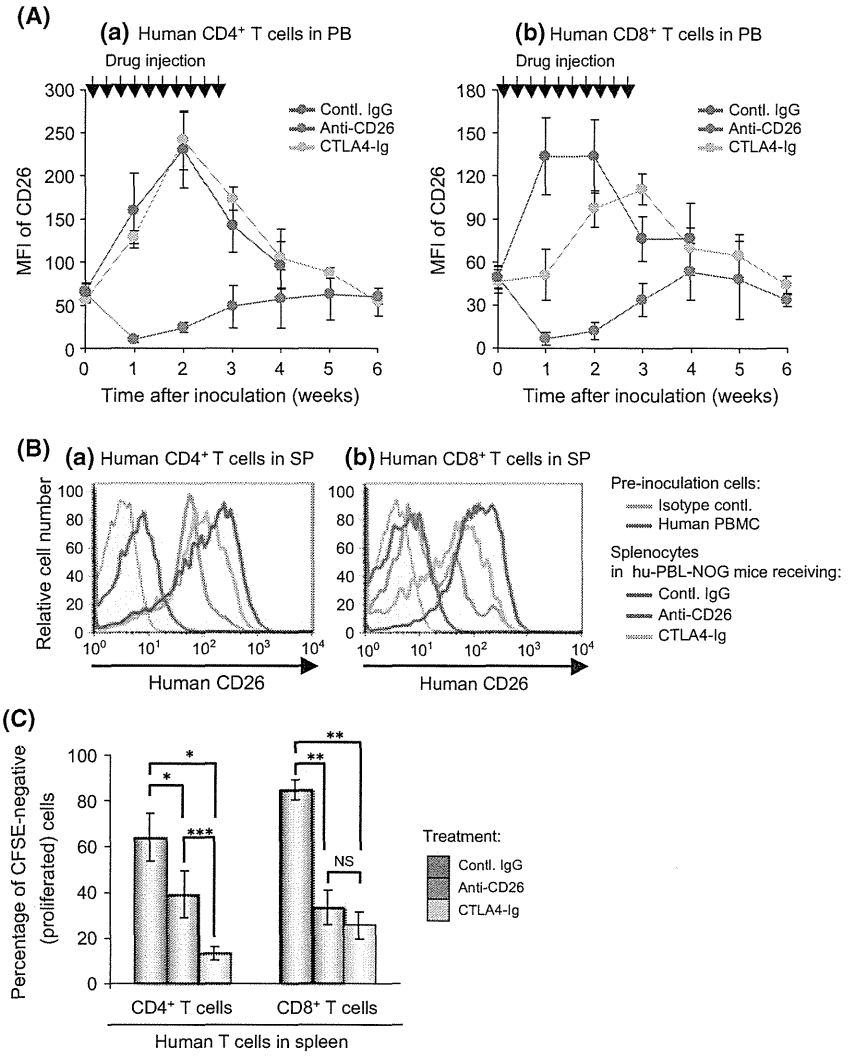

Fig 3. Anti-CD26 mAb treatment decreases CD26 expression of engrafted human lymphocytes in hu-PBL-NOG mice and decreases *in vivo* proliferation of $CD8^+$ T cells with preservation of $CD4^+$ T cell proliferation. Hu-PBL-NOG mice receiving humanized anti-CD26 mAb, CTLA4-Ig, or control IgG were bled every week. Red blood cells were then lysed, and PBMC subsets were analysed by flow cytometry. (A) Time course changes of mean fluorescence intensity (MFI) of human CD26 of peripheral blood (PB) in NOG mice receiving human PBMC plus control IgG (2 μg/dose, blue line, $n = 19$), anti-CD26 mAb (2 μg/dose, red line, $n = 24$), or CTLA4-Ig (2 μg/dose, green line, $n = 12$). MFI of human CD26 expression gated for human $CD4^+$ cells (panel a), or for human $CD8^+$ cells (panel b) is shown as average ± SD. (B) Representative histogram of human CD26 expression on day 14 of spleen cells (SP) in hu-PBL-NOG mice receiving control IgG (2 μg/dose, blue line, $n = 10$), anti-CD26 mAb (2 μg/dose, red line, $n = 10$), or CTLA4-Ig (2 μg/dose, green line, $n = 6$). Panel (a) shows representative human CD26 expression gated for human $CD4^+$ cells in murine splenocytes, and panel (b) shows human CD26 expression gated for human $CD8^+$ cells in splenocytes. Grey or brown line shows histogram of isotype control Ig staining, or human CD26 expression of human PBMC before inoculation, respectively. Similar results were observed in independent experiments using NOG mice receiving human PBMC plus control IgG ($n = 19$), anti-CD26 mAb ($n = 24$), or CTLA4-Ig ($n = 12$). (C) To analyse *in vivo* cell proliferation in hu-PBL-NOG mice, CFSE-labelled human PBMC were inoculated intraperitoneally into NOG mice, followed by injection of control IgG (2 μg/dose, blue bars, $n = 7$), anti-CD26 mAb (2 μg/dose, red bars, $n = 8$), or CTLA4-Ig (2 μg/dose, green bars, $n = 4$). Spleen cells from mice were harvested on day 7, and acquisition was performed using flow cytometry. Percentages of CFSE-negative, i.e., multiply dividing cells gated for human $CD4^+$ or $CD8^+$ cells, are shown as average ± SD *, ** or *** indicates $P < 0{\cdot}05$, NS denotes not significant.

Moreover, slight inflammation of the portal duct areas in the liver was observed in mice receiving CTLA4-Ig (Fig 4A, panels d, h, l). On the other hand, infiltration of human T cells in the liver was barely detected in mice receiving anti-CD26 mAb (Fig 4A panels c, g, k). In addition to the pathological changes seen in the liver, serum ALT activity was examined as another method of detecting GVHD-associated liver damage. Significant elevation of serum ALT activity was observed in mice receiving control IgG or CTLA4-Ig, while that of mice receiving anti-CD26 mAb was found to be near normal levels (Fig 4B, *). These data suggest that liver damage due to GVHD was suppressed in

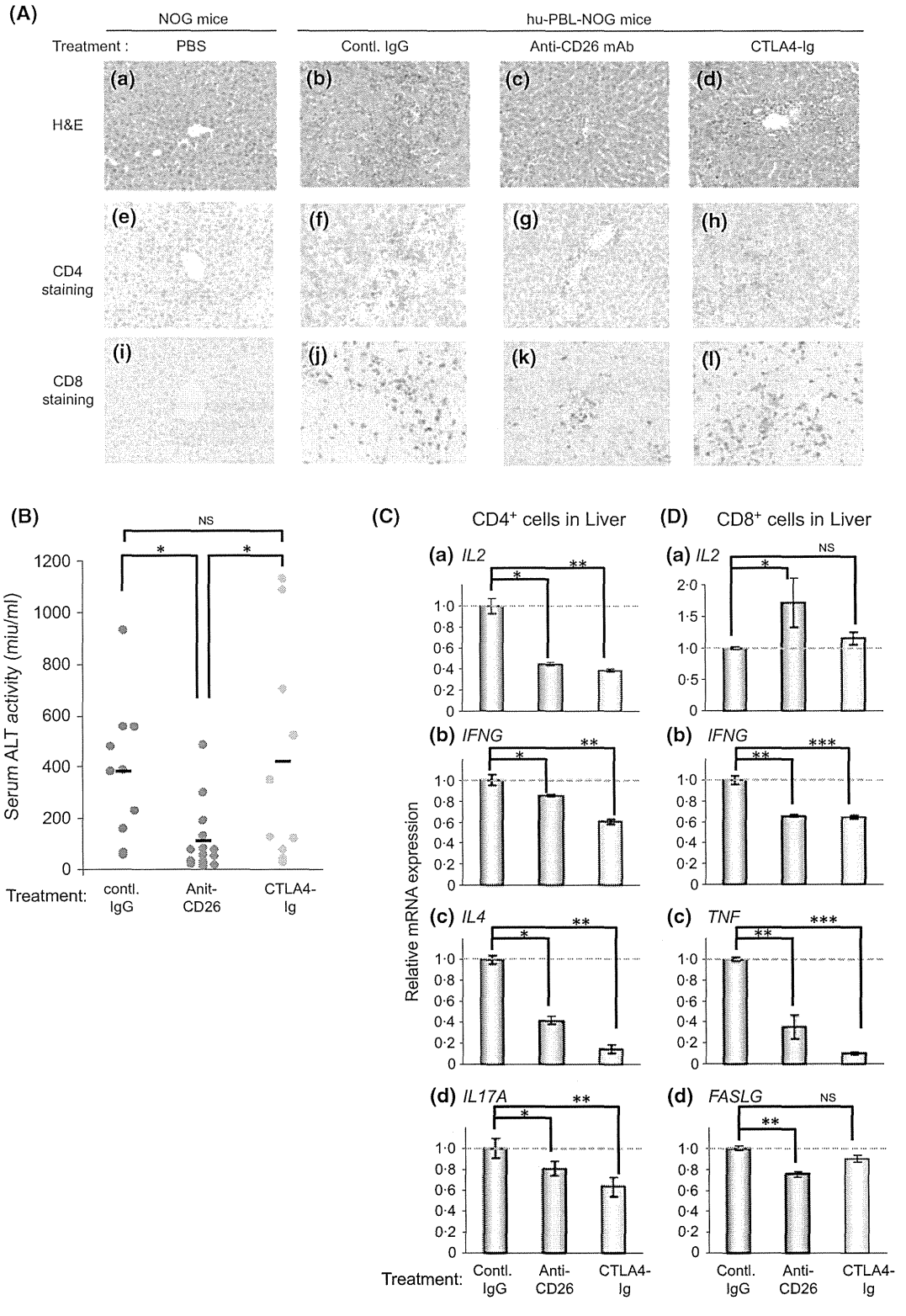

hu-PBL-NOG mice receiving anti-CD26 mAb, and that treatment with anti-CD26 mAb provided an advantage over CTLA4-Ig in preventing GVHD at similarly low doses. Along with lymphocyte infiltration in the GVHD target tissues, cytokine production level of donor-derived lymphocytes plays a role in tissue damages of the GVHD target organs (Shlomchik, 2007; Ferrara *et al*, 2009; Blazar *et al*, 2012). We therefore analysed the mRNA level of effector

Fig 4. Anti-CD26 mAb treatment in hu-PBL-NOG mice reduces liver infiltration of human lymphocytes with reduction of proinflammatory cytokines. (A) Representative examples of the liver on day 28 from NOG mice receiving PBS alone (negative control, panels a, e, i), or hu-PBL-NOG mice receiving control IgG (panels b, f, j), low dose anti-CD26 mAb (panels c, g, k), or low dose CTLA4-Ig (panels d, h, l). Slides were stained with H&E (panels a–d), anti-human CD4 (panels e–h), and anti-human CD8 (panels i–l). All slides are at 200× magnification. Similar results were observed in independent experiments using mice receiving PBS alone (n = 13), or hu-PBS-NOG mice receiving control IgG (n = 6), anti-CD26 mAb (n = 14), or CTLA4-Ig (n = 10). (B) Serum alanine transaminase (ALT) activity on day 21 in hu-PBL-NOG mice receiving control IgG (2 μg/dose, blue dots, n = 10), anti-CD26 mAb (2 μg/dose, red dots, n = 14), or CTLA4-Ig (2 μg/dose, green dots, n = 10). Each dot indicates an individual value and horizontal bars indicate mean value. * indicates $P < 0{\cdot}05$. NS denotes 'not significant'. (C) Human $CD4^+$ T cells were isolated from the liver of hu-PBL-NOG mice receiving control IgG (Contl. IgG, blue bars, n = 6), anti-CD26 mAb (red bars, n = 6), or CTLA4-Ig (green bars, n = 6) at 4 weeks after inoculation of human PBMCs. mRNA expression of human *IL2* (panel a), *IFNG* (panel b), *IL4* (panel c), or *IL17A* (panel d) was quantified by real-time RT-PCR, as described in Materials and methods. Each expression was normalized to hypoxanthine phosphoribosyltransferase 1 (*HPRT1*) and relative expression levels compared with the sample of control IgG treatment (indicated as dashed grey lines) were shown. * or ** indicates $P < 0{\cdot}05$, compared to control IgG. (D) mRNA levels of human $CD8^+$ T cells isolated from the liver of hu-PBL-NOG mice receiving control IgG (Contl. IgG, blue bars, n = 6), anti-CD26 mAb (red bars, n = 6), or CTLA4-Ig (green bars, n = 6) at 4 weeks after inoculation of human PBMCs are shown as in (C). mRNA expression of human *IL2* (panel a), *IFNG* (panel b), *TNF* (panel c), or *FASLG* (panel d) was quantified by real-time RT-PCR, as described in Materials and methods. The bar graphs are demonstrated as in (C). *, ** or *** indicates $P < 0{\cdot}05$, compared to control IgG. NS denotes 'not significant', compared to control IgG.

cytokines of donor-derived human $CD4^+$ or $CD8^+$ cells in the recipient liver. In hu-PBL-NOG mice receiving anti-CD26 mAb, levels of *IL2*, *IFNG*, *IL4* and *IL17A* of human $CD4^+$ cells isolated from the mouse liver decreased compared to those of hu-PBL-NOG mice receiving control IgG (in of Fig 4C, panels a–d, *). Similarly, treatment of hu-PBL-NOG mice with CTLA4-Ig resulted in lower levels of *IL2*, *IFNG*, *IL4* and *IL17A* of human $CD4^+$ cells isolated from mouse liver as compared to treatment with control IgG (Fig 4C, panels a–d, **). For human $CD8^+$ cells isolated from hu-PBL-NOG mice receiving anti-CD26 mAb, levels of *IFNG*, *TNF* and *FASLG* levels were decreased as compared to those of hu-PBL-NOG mice receiving control IgG (Fig 4D, panels b–d, **), while slight elevation of *IL2* was observed (Fig 4D, panel a, *). On the other hand, CTLA4-Ig-treated hu-PBL-NOG mice showed lower levels of *IFNG* and *TNF* as compared to control IgG-treated mice (Fig 4D, panels b and c,***), while *IL2* and *FASLG* production was at similar levels in the two groups (Fig 4D, panels a and d, NS). Taken together with the above data, these results indicate that anti-CD26 treatment in hu-PBL-NOG mice ameliorated liver GVHD by decreasing production of proinflammatory cytokines of donor-derived human lymphocytes as well as inhibiting lymphocyte infiltration in the liver, comparable to CTLA4-Ig.

GVL effect is maintained in hu-PBL-NOG mice receiving anti-CD26 mAb

Given that aGVHD and GVL effects are immune reactions that are highly linked to each other (Zorn *et al*, 2002; Wu & Ritz, 2009), we evaluated the potential influence of anti-CD26 mAb treatment on GVL effect. Prior to performing *in vivo* GVL experiments, we conducted mixed lymphocyte reaction assays to determine the cytotoxicity of human T cells on P815 leukaemic cells, and demonstrated that human $CD3^+$ T cells exerted *in vitro* cytotoxic effect on P815 cells (Fig S3A). For the subsequent animal studies, mice were injected subcutaneously in the flank with P815 leukaemic cells ($H2^d$) on day 0, followed by inoculation of human PBMCs and GVHD prophylaxis with anti-CD26 mAb or CTLA4-Ig. All NOG mice transplanted with P815 cells succumbed to leukaemia by 6 weeks of inoculation with progressive tumour enlargement (Fig 5A,B, grey lines; Fig S3B, panel a). Mice transplanted with P815 cells along with human PBMCs and control IgG showed minimal signs of tumour growth in the inoculated region, but all mice died around 4 weeks after inoculation (Fig 5A, blue line). Necropsies revealed that these mice died due to x-GVHD as manifested by the infiltration of human MNCs into the liver, spleen and lung (data not shown), suggesting that GVL effect was exerted in the presence of severe GVHD. On the other hand, mice inoculated with P815 along with human PBMC and anti-CD26 mAb exhibited enhanced survival rate with minimal evidence of GVHD (Fig 5A, red line). Importantly, mice in this group showed significantly slow initial tumour growth (Fig 5B, red line; Fig S3B, panel b), suggesting the preservation of GVL effect more than CTLA4-Ig treatment (Fig 5A, B, green lines).

When competent T cells are transferred into the recipients, allogeneic T cells have normal GVL capacity to eliminate leukaemic cells within 2 weeks after transplantation, while symptoms of GVHD become clinically obvious 3–4 weeks after transplantation (Meguro, 2010). Therefore, to further characterize the potential mechanisms involved in the preservation of GVL effect observed in hu-PBL-NOG mice receiving anti-CD26 mAb, we examined the expression level of effector cytokines of human $CD8^+$ T cells isolated from the spleens of hu-PBL-NOG mice at 2 weeks after transplantation. As shown in Fig 5C, the levels of *IL2* (panel a), *IFNG* (panel b), and *FASLG* (panel d) of human $CD8^+$ T cells was at comparable levels between hu-PBL-NOG mice receiving anti-CD26 mAb (red bars) and control IgG (blue bars), and the *TNF* level was increased in anti-CD26 mAb group compared to control IgG group (Fig 5C, panel c, *). On the other hand, CTLA4-Ig treatment suppressed the production

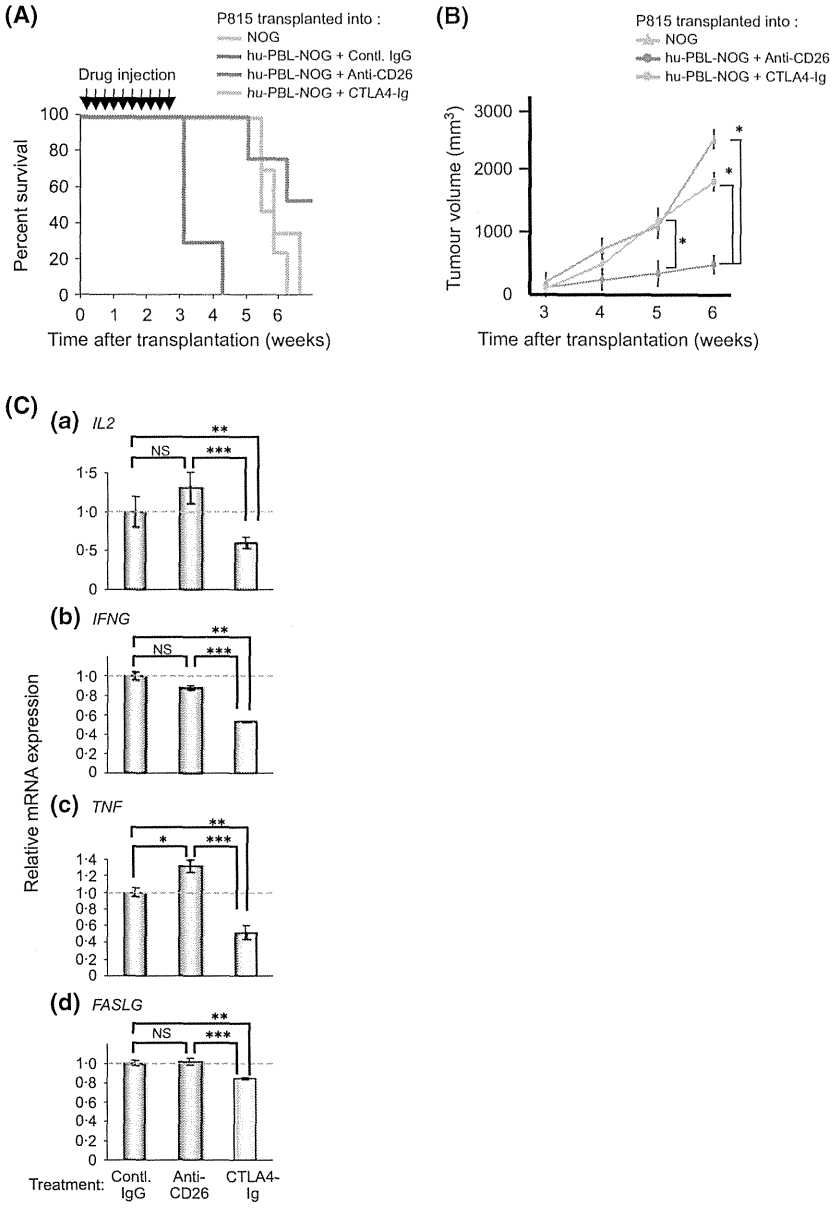

Fig 5. Anti-CD26 mAb treatment does not eliminate GVL activity. P815 leukaemic cells (2×10^4/body) were inoculated subcutaneously into the shaved flank of NOG mice. On the next day, human PBMCs (1×10^7/body) were inoculated intraperitoneally, followed by treatment with humanized anti-CD26 mAb, CTLA4-Ig, or control IgG (each, 2 μg/dose × 10 doses). (A) Kaplan–Meier survival curves for mice receiving P815 alone (grey line, $n = 4$), P815 plus PBMC plus control IgG (blue line, $n = 3$), P815 plus PBMC plus anti-CD26 mAb (red line, $n = 4$) or P815 plus PBMC plus CTLA4-Ig (green line, $n = 3$). (B) Tumour volume of P815 transplanted into the flank of NOG mice (grey line, $n = 4$), or hu-PBL-NOG mice receiving anti-CD26 mAb (red line, $n = 4$), or CTLA4-Ig (green line, $n = 3$). All mice receiving P815 plus PBMC plus control IgG (blue line of Fig 5A) died without tumour formation, therefore tumour volume of this group is not shown in the graph. * indicates $P < 0{\cdot}01$ of anti-CD26 mAb group versus P815 alone or control IgG groups. (C) Human $CD8^+$ T cells were isolated from the spleen of hu-PBL-NOG mice receiving control human IgG (Contl. IgG, $n = 4$), anti-CD26 mAb ($n = 4$), or CTLA4-Ig ($n = 3$) on day 14 after inoculation of human PBMCs. mRNA expression of human *IL2* (panel a), *IFNG* (panel b), *TNF* (panel c), or *FASLG* (panel d) was quantified by real-time RT-PCR. Each expression was normalized to *HPRT1* and relative expression levels compared with the sample of control IgG treatment (indicated dashed grey lines) were shown. *, ** or *** indicates $P < 0{\cdot}05$. NS denotes 'not significant'.

of *IL2*, *IFNG*, *TNF* and *FASLG* of human $CD8^+$ T cells in hu-PBL-NOG spleen as compared to control IgG or anti-CD26 mAb treatment (Fig 5C, ** and ***). These results suggest that the GVL effect of cytotoxic effector function occurring at the early time period prior to manifestation of x-GVHD was preserved with the associated increase in the production of *IL2*, *IFNG*, *TNF* or *FASLG* in hu-PBL-NOG mice receiving anti-CD26 mAb. On the other hand, in hu-PBL-NOG mice receiving CTLA4-Ig, proinflammatory cytokines produced from donor-derived $CD8^+$ cells suppressed any potential GVL effect at the early time period prior to x-GVHD development. These results suggest that CTLA4-Ig treatment suppressed the development of GVL as well as x-GVHD in hu-PBL-NOG mice, whereas effective GVL function was maintained with anti-CD26 mAb therapy.

$CD26^+$ MNCs infiltrate the skin or GI tract of alloHSCT patients with acute GVHD

Although treatment with a murine antibody against human CD26 exerted the therapeutic effect of controlling GVHD in patients with steroid-resistant acute GVHD following alloHSCT (Bacigalupo *et al*, 1985; de Meester *et al*, 1993), the precise cellular basis of human GVHD, as well as the role of CD26 in this process, has not yet been clearly delineated. To address this issue, we examined human GVHD tissue biopsies in alloHSCT recipients with or without active GVHD. Although the liver is one of the GVHD targeting organs, liver tissues are rarely obtained from patients with active hepatic GVHD in the clinical setting due to the risks of liver biopsies. Pathological diagnosis is typically conducted

with endoscopic GI tract mucosal biopsy for GI GVHD (Kreisel *et al*, 2011), as well as skin biopsy for the diagnosis of skin GVHD (Sale *et al*, 1977). Therefore, we evaluated specimens from skin biopsies and endoscopic samples of upper GI (duodenal) mucosa harvested from patients with active GVHD patients. Thirty-four adult patients (median age, 38 years; range, 22–60 years) with AML who underwent alloHSCT at the Keio University Hospital were included in this study. GVHD prophylaxis was ciclosporin and methotrexate for related donor transplantation, or tacrolimus and methotrexate for unrelated donor transplantation. The demographic profiles of the biopsied patients are shown in Table I. All 34 patients had clinical skin GVHD (Stage I, $n = 16$; Stage II, $n = 11$; Stage III, $n = 7$). Skin biopsies from 34 patients were analysed for $CD26^+$ MNC infiltration. Staining of human skin biopsies for CD26 revealed that all patients with active GVHD had $CD26^+$ MNC infiltration in the skin (Fig 6A, panels a–c). To determine that $CD26^+$ MNCs are $CD3^+$ T cells, co-staining of a representative skin specimen revealed that $CD3^+CD26^+$ MNCs infiltrated the skin of patients with aGVHD (Fig. S4). Fig 6B demonstrates data correlating the absolute number (per square millimetre) of $CD26^+$ MNCs in the skin with the GVHD pathological grade, and reveals that the level of $CD26^+$ MNCs constitutively infiltrating the skin of patients with aGVHD did not correlate with disease severity. Furthermore, among patients who had biopsies of the upper GI tract mucosa performed as a diagnostic procedure for digestive symptoms, 32 patients had clinical GI GVHD (Stage I, $n = 10$; Stage II, $n = 14$; Stage III, $n = 7$; Stage IV, $n = 1$). Staining of human duodenal mucosal biopsies for CD26 revealed that all patients with active GVHD had $CD26^+$ MNC infiltration in the duodenal mucosa (Fig 6C, panels a–c). In addition, the absolute number (per square millimetre) of $CD26^+$ MNCs constitutively infiltrating the duodenal mucosa of patients with aGVHD did not correlate with disease severity as indicated by GVHD pathologic grade (Fig 6D). However, in patients with severe GVHD, $CD26^+$ MNCs were found to infiltrate into the stromal tissue of the duodenum, and were not only limited to the surface mucosa (Fig 6C, panel c). Taken together, these results strongly suggest that $CD26^+$ MNCs play an important role in the inflamed tissues of aGVHD patients, consistent with previous data demonstrating that $CD26^+$ lymphocytes migrated to inflamed tissues with effector functions (Eguchi *et al*, 1989; Gerli *et al*, 1996; Hafler *et al*, 1985; Mizokami *et al*, 1996), suggesting that CD26 is a logical therapeutic target in aGVHD.

Table I. Patients characteristics and clinical status at time of biopsy for diagnosis of acute GVHD.

Disease (*n*)	
AML	34
1st or 2nd CR	24
Advanced	10
Age (years)	
Median	38
Range	22–60
Gender (*n*)	
Male	20
Female	14
Allo-graft source (*n*)	
BM	30
PB	1
CB	3
Conditioning (*n*)	
Full	25
Reduced	9
Matching (*n*)	
Related	8
Unrelated	26
*aGVHD clinical grade (*n*)	
0	6
I	10
II	9
III	8
IV	1

*aGVHD, acute graft-versus-host disease; AML, acute myeloid leukaemia; BM, bone marrow; CB, cord blood; CR, complete remission; PB, peripheral blood.

Discussion

In the current study, we show that $CD26^+$ T cells play an important role in GVHD mediated by human lymphocytes, and that anti-CD26 mAb is an effective treatment for GVHD in hu-PBL-NOG mouse model. The effect of anti-CD26 mAb on GVHD is shown to be comparable to the clinically available costimulation blocking agent, CTLA4-Ig (abatacept). Importantly, anti-CD26 mAb therapy appears to be superior to CTLA4-Ig treatment in that it preserves engraftment and the GVL effect. Finally, our work demonstrates significant infiltration of $CD26^+$ MNCs in GVHD target tissues obtained from patients with aGVHD.

Our present work indicates the infiltration of human $CD26^+$ lymphocytes in the x-GVHD lesions of hu-PBL-NOG mice (Fig 1B) and the presence of human $CD26^{high}$ T cells in the peripheral blood or spleen of hu-PBL-NOG mice that developed x-GVHD (Fig 3A,B). When x-GVHD of hu-PBL-NOG mice was diminished by anti-CD26 mAb treatment, $CD26^{high}$ T cells were not detected in the peripheral blood and spleen (Fig 3A,B). A potential explanation for this finding may be internalization of surface CD26 expression on the inoculated human lymphocytes induced by humanized anti-CD26 mAb therapy (Dang *et al*, 1990). The decreased $CD26^{high}$ lymphocyte level, with resultant decline in CD26-mediated costimulation and migration, might contribute to lowered xenogeneic activation and decreased tissue infiltration of GVHD target organs. In fact, a low level of lymphocyte infiltration in the liver was shown in hu-PBL-NOG mice receiving a low dose of CTLA4-Ig (Fig 4A, panels d, h, l), while lymphocyte infiltration in the liver was barely detected

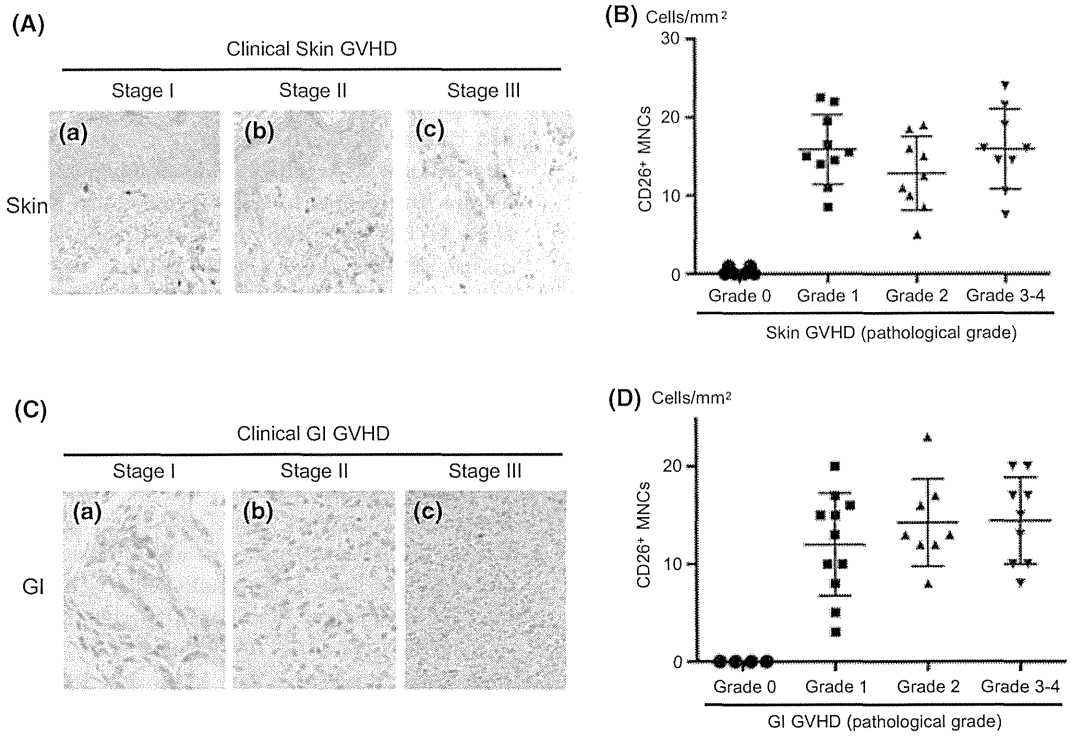

Fig 6. CD26$^+$ MNCs infiltrate into the skin or duodenal mucosa of alloHSCT patients with acute GVHD. Histopathological evaluation of representative skin and duodenal mucosa samples biopsied from transplant patients and stained with anti-human CD26 polyclonal antibody, counterstained with haematoxylin, and then analysed in a blinded fashion, as described in Materials and methods. (A) Representative examples of skin obtained from patients with clinical Stage I (panel a), Stage II (panel b), or Stage III (panel c) of acute skin GVHD. Original magnification 100×. (B) Graphs comparing the relative amount of CD26$^+$ MNCs in the skin with acute GVHD pathologic grade 0 (n = 6), 1 (n = 10), 2 (n = 9), or 3–4 (n = 9). Each dot indicates individual value. The horizontal lines in the scattergrams indicate each mean value, and error bars indicate SD. (C) Representative examples of duodenal mucosa obtained from patients with gastrointestinal (GI) clinical Stage I (panel a), Stage II (panel b), or Stage III (panel c) of acute GVHD. Original magnification 100×. CD26$^+$ MNCs infiltrated locally in the mucosal epithelia, while for patients with Stage III, increasing number of CD26$^+$ MNCs was observed in the interstitial tissue as well as in the mucosal epithelia. (D) Graphs comparing the relative amount of CD26$^+$ MNCs in the duodenal mucosa with acute GVHD pathological grade 0 (n = 4), 1 (n = 11), 2 (n = 8), or 3–4 (n = 9). Each dot indicates individual value. The horizontal lines in the scattergrams indicate each mean value, and error bars indicate SD.

in hu-PBL-NOG mice receiving anti-CD26 mAb (Fig 4A, panels c, g, k). These observations might result from the fact that CTLA4 has no direct effect on lymphocyte migration, whereas the CD26 molecule is strongly associated with lymphocyte migration into inflamed tissues (Hafler *et al*, 1985; Eguchi *et al*, 1989; Masuyama *et al*, 1992; Gerli *et al*, 1996; Mizokami *et al*, 1996). It is also possible that anti-CD26 mAb treatment could affect other functional programming of inoculated human lymphocytes, such as cell cycle regulation. We have previously reported that binding of anti-CD26 mAb to CD26 on T cell surface inhibits human T cell growth and proliferation in both CD26-transfected Jurkat T-cell lines and human T cell clones by inducing G1/S arrest, which is associated with enhancement of $p21^{Cip1}$ (CDKN1A) expression (Ohnuma *et al*, 2002). In this regard, the suppression of x-GVHD by anti-CD26 mAb shown here might result from a direct effect on cell cycle inhibition mediated by anti-CD26 mAb. In addition to the preventive effect on x-GVHD of anti-CD26 mAb, we observed that systemic manifestations of x-GVHD were greatly reduced by administration of anti-CD26 mAb when x-GVHD symptoms developed after 4 weeks of human PBMCs inoculation (data not shown). Taken together, our results indicate that anti-CD26 mAb treatment appears to affect T cell functions of inoculated human lymphocytes in hu-PBL-NOG mice.

Costimulatory pathways are necessary to induce T cell proliferation, cytokine secretion and effector function following antigen-mediated T cell receptor activation. Given that CD28 is widely expressed on T cells and CD28$^-$CD8$^+$ T cells are well-recognized as naïve or highly-antigen experienced (late-differentiated) cells (Rudd *et al*, 2009; Strioga *et al*, 2011), blockade of CD28 pathway may lead to profound suppression of T cell function. In fact, our current study showed that T cell proliferation or cytokine production was inhibited at a greater level by CTLA4-Ig than by anti-CD26 mAb (Figs 3C, 4C, 4D or 5C). In this regard, immunosuppression by CTLA4-Ig not only diminished the engraftment of donor-derived human lymphocytes in NOG mice

(Fig 2C), but also decreased the GVL effect in hu-PBL-NOG mice (Fig 5A,B, green lines). These data strongly suggest that while CTLA4-Ig exhibits strong suppressive effect on x-GVHD, it also has several adverse effects, such as graft rejection, inhibition of GVL reactivity or enhancement of opportunistic infections.

Our previous studies showed that CD26-mediated costimulation in human $CD4^+$ T cells exerted an effect on production of T_H1 type proinflammatory cytokines such as IL2 or IFNG (Morimoto & Schlossman, 1998), and that soluble anti-CD26 mAb treatment decreased IL2 production of human $CD4^+$ T cells (Ohnuma *et al*, 2002). Our present data indicate that anti-CD26 mAb treatment suppressed the generation of *IL2* and *IFNG* of donor-derived human $CD4^+$ cells in the liver of hu-PBL-NOG mice (Fig 4C, panels a, b), and that this suppression might result in the inhibition of x-GVHD. In addition to T_H1 type cytokines, the T_H2 type cytokine IL4 was found to be abundant in GVHD liver lesions in human studies, and a high level of IL4 production in the GVHD liver tissue appears to contribute to its pathogenesis (Lai *et al*, 2012). In agreement with previous studies of patients with aGVHD (Lai *et al*, 2012), we observed the reduction of *IL4* production of donor-derived human $CD4^+$ T cells in the liver of hu-PBL-NOG mice receiving anti-CD26 mAb or CTLA4-Ig (Fig 4C, panel c). Recently, it was reported that $CD26^{high}$ T cells contain T_H17 cells, and that $CD26^{high}$ T_H17 cells are enriched in the inflamed tissue of patients with hepatitis and inflammatory bowel disease (Bengsch *et al*, 2012). We observed decrease in the production of *IL17A* in hu-PBL-NOG mice treated with anti-CD26 mAb or CTLA4-Ig (Fig 4C, panel d). Our present data on cytokine production suggest that, due to the paradoxical and variable effects resulting from targeting T_H1-, T_H2- and T_H17-type cytokines, such approaches alone may not be sufficient to fully treat or prevent GVHD in the clinical setting, but they may serve as useful adjunct therapeutic strategies to reduce GVHD-associated tissue injuries.

Recently, it has been reported that $CD8^+$ T cells specific for influenza express high levels of CD26, and that this subset could produce IL2 following stimulation, while $CD8^+$ T cells specific for chronic infection with persistent antigens, such as cytomegalovirus (CMV), Epstain-Barr virus (EBV) or human immunedeficiency virus (HIV), lack CD26 expression (Ibegbu *et al*, 2009). The authors concluded that high CD26 expression among $CD8^+$ T cells may be a marker of effective long-term memory T cell formation and that the lack of CD26 expression among $CD8^+$ T cells in CMV, EBV or HIV infection may indicate defective memory T cells (Ibegbu *et al*, 2009). It is therefore a concern that anti-CD26 mAb therapy may potentially cause increased infection. However, $CD8^+$ T cells in hu-PBL-NOG mice treated with anti-CD26 mAb exhibited increased *IL2* production (Fig 4D, panel a; Fig 5C, panel a). These results strongly suggest that IL2-producing $CD8^+$ T cells persist despite humanized anti-CD26 mAb therapy, which may lead to the formation of effective memory T cells against potential opportunistic infections following alloHSCT. In addition, IL2 is necessary for the proliferation of regulatory T cells (Treg), which can ameliorate GVHD (Koreth *et al*, 2011). Therefore, our data that IL2-producing $CD8^+$ T cells still remain following humanized anti-CD26 mAb therapy may indicate the existence of immune tolerance via Treg proliferation in the GVHD target organs.

Results from murine GVHD models have not always translated to human disease and discrepancies between murine and human samples have been reported. While the CD26 amino acid sequence has 85% amino acid identity with the mouse CD26 (Marguet *et al*, 1992), mouse CD26 exerts no costimulatory function in mouse T cells, and is not an activation marker of T cells nor an adenosine deaminase-binding protein (Marguet *et al*, 1992; Yan *et al*, 2003). On the other hand, caveolin-1 (CAV1), a costimulatory ligand for CD26 in humans, has 95% amino acid identity with the mouse caveolin-1 (Engelman *et al*, 1998), and the binding regions of the mouse caveolin-1 for human CD26 are well conserved. Therefore, human T cells were activated even in NOG mice via CD26-caveolin-1 interaction. Another important point to consider when interpreting our data is the fact that, in our studies, mice were analysed at a time when they were moribund, in contrast to the samples obtained from patients that, for the most part, were obtained at the time of GVHD diagnosis or shortly thereafter. Moreover, first-line therapies for clinical GVHD, such as methotrexate or calcineurin inhibitors, may have an effect on T cell costimulatory signalling, cytokine production or expression of cell surface molecules.

Specific inhibition of DPP4 enzyme via Diprotin A enhanced bone marrow engraftment in certain murine BMT models (Christopherson *et al*, 2004). Although DPP4 enzymatic activity is required for CD26-mediated T cell costimulation (Morimoto & Schlossman, 1998), it is unclear whether DPP4 enzyme inhibition has an effect on GVHD development. Regarding this point, we note that the humanized anti-CD26 mAb used in the present study does not inhibit DPP4 enzymatic activity of human CD26 (data not shown).

In conclusion, CD26-mediated T cell activation appears to play a significant role in human GVHD. As full suppression of x-GVHD with interventional therapies is currently a difficult challenge, our data demonstrating that control of x-GVHD can be achieved by modulating $CD26^{high}$ T cells with anti-CD26 mAb are potentially important clinically. Our work also suggests that anti-CD26 mAb treatment may be a novel therapeutic approach for GVHD in the future.

Acknowledgements

The authors thank Ms Kaoru Komoriya for excellent assistance with animal husbandry. This work was supported by Grant-in-Aid of The Ministry of Education, Science, Sports (K.O. and C.M.) and Culture, Ministry of Health, Labour, and Welfare, Japan (C.M.).

Authorship contributions

Contributions: R.H., and J.Y. performed the experiments, interpreted the data and assisted with the paper, K.O. and C.M. designed the research, interpreted the data and wrote the paper, N.H.D. interpreted the data, assisted with the paper, and proof-read the manuscript, and T.Y. provided the clinical data and samples, performed the experiments, analysed pathological results, interpreted the data and assisted with the paper.

Conflict-of-interest disclosure

The authors declare no competing financial interests.

Supporting Information

Additional Supporting Information may be found in the online version of this article:

Fig S1. Mouse anti-human CD26 mAb clone 5K78 recognizes human CD26 even in the presence of humanized anti-CD26 mAb.

Fig S2. Human $CD3^+CD26^+$ T cells infiltrated the liver of hu-PBL-NOG mice developing x-GVHD.

Fig S3. GVL experiments in hu-PBL-NOG mice.

Fig S4. $CD3^+CD26^+$ MNCs infiltrate the skin of alloHSCT patients with acute GVHD.

Table SI. The primer sequences for RT-PCR.

References

Aoe, K., Amatya, V.J., Fujimoto, N., Ohnuma, K., Hosono, O., Hiraki, A., Fujii, M., Yamada, T., Dang, N.H., Takeshima, Y., Inai, K., Kishimoto, T. & Morimoto, C. (2012) CD26 overexpression is associated with prolonged survival and enhanced chemosensitivity in malignant pleural mesothelioma. *Clinical Cancer Research*, **18**, 1447–1456.

Bacigalupo, A., Corte, G., Ramarli, D., van Lint, M.T., Frassoni, F. & Marmont, A. (1985) Intravenous monoclonal antibody (BT 5/9) for the treatment of acute graft-versus-host disease. *Acta Haematologica*, **73**, 185–186.

Bengsch, B., Seigel, B., Flecken, T., Wolanski, J., Blum, H.E. & Thimme, R. (2012) Human Th17 cells express high levels of enzymatically active dipeptidylpeptidase IV (CD26). *Journal of Immunology*, **188**, 5438–5447.

Blazar, B.R., Taylor, P.A., Boyer, M.W., Panoskaltsis-Mortari, A., Allison, J.P. & Vallera, D.A. (1997) CD28/B7 interactions are required for sustaining the graft-versus-leukemia effect of delayed post-bone marrow transplantation splenocyte infusion in murine recipients of myeloid or lymphoid leukemia cells. *Journal of Immunology*, **159**, 3460–3473.

Blazar, B.R., Murphy, W.J. & Abedi, M. (2012) Advances in graft-versus-host disease biology and therapy. *Nature Reviews Immunology*, **12**, 443–458.

Briones, J., Novelli, S. & Sierra, J. (2011) T-cell costimulatory molecules in acute-graft-versus host disease: therapeutic implications. *Bone Marrow Research*, **2011**, 976793.

Christopherson, K.W. II, Hangoc, G., Mantel, C.R. & Broxmeyer, H.E. (2004) Modulation of hematopoietic stem cell homing and engraftment by CD26. *Science*, **305**, 1000–1003.

Dang, N.H., Torimoto, Y., Sugita, K., Daley, J.F., Schow, P., Prado, C., Schlossman, S.F. & Morimoto, C. (1990) Cell surface modulation of CD26 by anti-1F7 monoclonal antibody. Analysis of surface expression and human T cell activation. *Journal of Immunology*, **145**, 3963–3971.

Dong, R.P., Tachibana, K., Hegen, M., Scharpe, S., Cho, D., Schlossman, S.F. & Morimoto, C. (1998) Correlation of the epitopes defined by anti-CD26 mAbs and CD26 function. *Molecular Immunology*, **35**, 13–21.

Eguchi, K., Ueki, Y., Shimomura, C., Otsubo, T., Nakao, H., Migita, K., Kawakami, A., Matsunaga, M., Tezuka, H., Ishikawa, N., Ito, K. & Nagataki, S. (1989) Increment in the $Ta1^+$ cells in the peripheral blood and thyroid tissue of patients with Graves' disease. *Journal of Immunology*, **142**, 4233–4240.

Engelman, J.A., Zhang, X., Galbiati, F., Volonte, D., Sotgia, F., Pestell, R.G., Minetti, C., Scherer, P.E., Okamoto, T. & Lisanti, M.P. (1998) Molecular genetics of the caveolin gene family: implications for human cancers, diabetes, Alzheimer disease, and muscular dystrophy. *American Journal of Human Genetics*, **63**, 1578–1587.

Ferrara, J.L., Levine, J.E., Reddy, P. & Holler, E. (2009) Graft-versus-host disease. *Lancet*, **373**, 1550–1561.

Fox, D.A., Hussey, R.E., Fitzgerald, K.A., Acuto, O., Poole, C., Palley, L., Daley, J.F., Schlossman, S.F. & Reinherz, E.L. (1984) Ta1, a novel 105 KD human T cell activation antigen defined by a monoclonal antibody. *Journal of Immunology*, **133**, 1250–1256.

Genovese, M.C., Becker, J.C., Schiff, M., Luggen, M., Sherrer, Y., Kremer, J., Birbara, C., Box, J., Natarajan, K., Nuamah, I., Li, T., Aranda, R., Hagerty, D.T. & Dougados, M. (2005) Abatacept for rheumatoid arthritis refractory to tumor necrosis factor alpha inhibition. *New England Journal of Medicine*, **353**, 1114–1123.

Gerli, R., Muscat, C., Bertotto, A., Bistoni, O., Agea, E., Tognellini, R., Fiorucci, G., Cesarotti, M. & Bombardieri, S. (1996) CD26 surface molecule involvement in T cell activation and lymphokine synthesis in rheumatoid and other inflammatory synovitis. *Clinical Immunology and Immunopathology*, **80**, 31–37.

Giralt, S. (2012) Graft-versus-host disease: have we solved the problem? *Journal of Clinical Oncology*, **30**, 3160–3161.

Gribben, J.G., Guinan, E.C., Boussiotis, V.A., Ke, X.Y., Linsley, L., Sieff, C., Gray, G.S., Freeman, G.J. & Nadler, L.M. (1996) Complete blockade of B7 family-mediated costimulation is necessary to induce human alloantigen-specific anergy: a method to ameliorate graft-versus-host disease and extend the donor pool. *Blood*, **87**, 4887–4893.

Hafler, D.A., Fox, D.A., Manning, M.E., Schlossman, S.F., Reinherz, E.L. & Weiner, H.L. (1985) *In vivo* activated T lymphocytes in the peripheral blood and cerebrospinal fluid of patients with multiple sclerosis. *New England Journal of Medicine*, **312**, 1405–1411.

Hatano, R., Ohnuma, K., Yamamoto, J., Dang, N.H. & Morimoto, C. (2013) CD26-mediated co-stimulation in human $CD8^+$ T cells provokes effector function via pro-inflammatory cytokine production. *Immunology*, **138**, 165–172.

Ibegbu, C.C., Xu, Y.X., Fillos, D., Radziewicz, H., Grakoui, A. & Kourtis, A.P. (2009) Differential expression of CD26 on virus-specific $CD8^+$ T cells during active, latent and resolved infection. *Immunology*, **126**, 346–353.

Ito, M., Hiramatsu, H., Kobayashi, K., Suzue, K., Kawahata, M., Hioki, K., Ueyama, Y., Koyanagi, Y., Sugamura, K., Tsuji, K., Heike, T. & Nakahata, T. (2002) NOD/SCID/γ_c^{null} mouse: an excellent recipient mouse model for engraftment of human cells. *Blood*, **100**, 3175–3182.

Koreth, J., Matsuoka, K., Kim, H.T., McDonough, S.M., Bindra, B., Alyea, E.P. 3rd, Armand, P., Cutler, C., Ho, V.T., Treister, N.S., Bienfang, D.C., Prasad, S., Tzachanis, D., Joyce, R.M., Avigan, D.E., Antin, J.H., Ritz, J. & Soiffer, R.J. (2011) Interleukin-2 and regulatory T cells in graft-versus-host disease. *New England Journal of Medicine*, **365**, 2055–2066.

Kreisel, W., Dahlberg, M., Bertz, H., Harder, J., Potthoff, K., Deibert, P., Schmitt-Graeff, A. & Finke, J. (2011) Endoscopic diagnosis of acute intestinal GVHD following allogeneic hematopoietic SCT: a retrospective analysis in 175 patients. *Bone Marrow Transplantation*, **47**, 430–438.

Lai, H.Y., Chou, T.Y., Tzeng, C.H. & Lee, O.K. (2012) Cytokine profiles in various graft-versus-

host disease target organs following hematopoietic stem cell transplantation. *Cell Transplantation*, **21**, 2033–2045.

Lenschow, D.J., Zeng, Y., Thistlethwaite, J.R., Montag, A., Brady, W., Gibson, M.G., Linsley, P.S. & Bluestone, J.A. (1992) Long-term survival of xenogeneic pancreatic islet grafts induced by CTLA4Ig. *Science*, **257**, 789–792.

Marguet, D., Bernard, A.M., Vivier, I., Darmoul, D., Naquet, P. & Pierres, M. (1992) cDNA cloning for mouse thymocyte-activating molecule. A multifunctional ecto-dipeptidyl peptidase IV (CD26) included in a subgroup of serine proteases. *Journal of Biological Chemistry*, **267**, 2200–2208.

Masuyama, J., Berman, J.S., Cruikshank, W.W., Morimoto, C. & Center, D.M. (1992) Evidence for recent as well as long term activation of T cells migrating through endothelial cell monolayers *in vitro*. *Journal of Immunology*, **148**, 1367–1374.

de Meester, I., Scharpe, S., Vanham, G., Bosmans, E., Heyligen, H., Vanhoof, G. & Corte, G. (1993) Antibody binding profile of purified and cell-bound CD26. Designation of BT5/9 and TA5.9 to the CD26 cluster. *Immunobiology*, **188**, 145–158.

Meguro, A. (2010) Lack of IL-21 signal attenuates graft-versus-leukemia effect in the absence of CD8 T-cells. *Bone Marrow Transplantation*, **46**, 1557–1565.

Mizokami, A., Eguchi, K., Kawakami, A., Ida, H., Kawabe, Y., Tsukada, T., Aoyagi, T., Maeda, K., Morimoto, C. & Nagataki, S. (1996) Increased population of high fluorescence 1F7 (CD26) antigen on T cells in synovial fluid of patients with rheumatoid arthritis. *Journal of Rheumatology*, **23**, 2022–2026.

Morimoto, C. & Schlossman, S.F. (1998) The structure and function of CD26 in the T-cell immune response. *Immunological Reviews*, **161**, 55–70.

Morimoto, C., Torimoto, Y., Levinson, G., Rudd, C.E., Schrieber, M., Dang, N.H., Letvin, N.L. & Schlossman, S.F. (1989) 1F7, a novel cell surface molecule, involved in helper function of CD4 cells. *Journal of Immunology*, **143**, 3430–3439.

Muscat, C., Bertotto, A., Agea, E., Bistoni, O., Ercolani, R., Tognellini, R., Spinozzi, F., Cesarotti, M. & Gerli, R. (1994) Expression and functional role of 1F7 (CD26) antigen on peripheral blood and synovial fluid T cells in rheumatoid arthritis patients. *Clinical and Experimental Immunology*, **98**, 252–256.

Ohnuma, K., Ishii, T., Iwata, S., Hosono, O., Kawasaki, H., Uchiyama, M., Tanaka, H., Yamochi, T., Dang, N.H. & Morimoto, C. (2002) G1/S cell cycle arrest provoked in human T cells by antibody to CD26. *Immunology*, **107**, 325–333.

Ohnuma, K., Dang, N.H. & Morimoto, C. (2008) Revisiting an old acquaintance: CD26 and its molecular mechanisms in T cell function. *Trends in Immunology*, **29**, 295–301.

Pasquini, M.C., Wang, Z., Horowitz, M.M. & Gale, R.P. (2010) 2010 report from the Center for International Blood and Marrow Transplant Research (CIBMTR): current uses and outcomes of hematopoietic cell transplants for blood and bone marrow disorders. *Clinical Transplants*, **2010**, 87–105.

Przepiorka, D., Weisdorf, D., Martin, P., Klingemann, H.G., Beatty, P., Hows, J. & Thomas, E.D. (1995) 1994 consensus conference on acute GVHD grading. *Bone Marrow Transplantation*, **15**, 825–828.

Rudd, C.E., Taylor, A. & Schneider, H. (2009) CD28 and CTLA-4 coreceptor expression and signal transduction. *Immunological Reviews*, **229**, 12–26.

Saito, K. (1998) Involvement of CD40 ligand-CD40 and CTLA4-B7 pathways in murine acute graft-versus-host disease induced by allogeneic T cells lacking CD28. *J. Immunol.*, **160**, 4225–4231.

Sale, G.E., Lerner, K.G., Barker, E.A., Shulman, H.M. & Thomas, E.D. (1977) The skin biopsy in the diagnosis of acute graft-versus-host disease in man. *American Journal of Pathology*, **89**, 621–636.

Shlomchik, W.D. (2007) Graft-versus-host disease. *Nature Reviews Immunology*, **7**, 340–352.

Strioga, M., Pasukoniene, V. & Characiejus, D. (2011) $CD8^+CD28^-$ and $CD8^+CD57^+$ T cells and their role in health and disease. *Immunology*, **134**, 17–32.

Tanaka, T., Camerini, D., Seed, B., Torimoto, Y., Dang, N.H., Kameoka, J., Dahlberg, H.N., Schlossman, S.F. & Morimoto, C. (1992) Cloning and functional expression of the T cell activation antigen CD26. *Journal of Immunology*, **149**, 481–486.

Tsirigotis, P., Or, R., Resnick, I.B. & Shapira, M.Y. (2012) Immunotherapeutic approaches to improve graft-versus-tumor effect and reduce graft-versus-host disease. *Immunotherapy*, **4**, 407–424.

Vincenti, F., Charpentier, B., Vanrenterghem, Y., Rostaing, L., Bresnahan, B., Darji, P., Massari, P., Mondragon-Ramirez, G.A., Agarwal, M., Di Russo, G., Lin, C.S., Garg, P. & Larsen, C.P. (2010) A phase III study of belatacept-based immunosuppression regimens versus cyclosporine in renal transplant recipients (BENEFIT study). *American Journal of Transplantation*, **10**, 535–546.

Washington, K. & Jagasia, M. (2009) Pathology of graft-versus-host disease in the gastrointestinal tract. *Human Pathology*, **40**, 909–917.

Wu, C.J. & Ritz, J. (2009) Revealing tumor immunity after hematopoietic stem cell transplantation. *Clinical Cancer Research*, **15**, 4515–4517.

Yan, S., Marguet, D., Dobers, J., Reutter, W. & Fan, H. (2003) Deficiency of CD26 results in a change of cytokine and immunoglobulin secretion after stimulation by pokeweed mitogen. *European Journal of Immunology*, **33**, 1519–1527.

Zorn, E., Wang, K.S., Hochberg, E.P., Canning, C., Alyea, E.P., Soiffer, R.J. & Ritz, J. (2002) Infusion of $CD4^+$ donor lymphocytes induces the expansion of $CD8^+$ donor T cells with cytolytic activity directed against recipient hematopoietic cells. *Clinical Cancer Research*, **8**, 2052–2060.

PLOS ONE

Nuclear Localization of CD26 Induced by a Humanized Monoclonal Antibody Inhibits Tumor Cell Growth by Modulating of POLR2A Transcription

Kohji Yamada[1], Mutsumi Hayashi[1], Hiroko Madokoro[1], Hiroko Nishida[1], Wenlin Du[1], Kei Ohnuma[2], Michiie Sakamoto[1], Chikao Morimoto[2], Taketo Yamada[1]*

1 Department of Pathology, School of Medicine, Keio University, Shinjuku-ku, Tokyo, Japan, **2** Department of Therapy Development and Innovation for Immune Disorders and Cancers, Graduate School of Medicine, Juntendo University, Bunkyo-ku, Tokyo, Japan

Abstract

CD26 is a type II glycoprotein known as dipeptidyl peptidase IV and has been identified as one of the cell surface markers associated with various types of cancers and a subset of cancer stem cells. Recent studies have suggested that CD26 expression is involved in tumor growth, tumor invasion, and metastasis. The CD26 is shown in an extensive intracellular distribution, ranging from the cell surface to the nucleus. We have previously showed that the humanized anti-CD26 monoclonal antibody (mAb), YS110, exhibits inhibitory effects on various cancers. However, functions of CD26 on cancer cells and molecular mechanisms of impaired tumor growth by YS110 treatment are not well understood. In this study, we demonstrated that the treatment with YS110 induced nuclear translocation of both cell-surface CD26 and YS110 in cancer cells and xenografted tumor. It was shown that the CD26 and YS110 were co-localized in nucleus by immunoelectron microscopic analysis. In response to YS110 treatment, CD26 was translocated into the nucleus via caveolin-dependent endocytosis. It was revealed that the nuclear CD26 interacted with a genomic flanking region of the gene for POLR2A, a subunit of RNA polymerase II, using a chromatin immunoprecipitation assay. This interaction with nuclear CD26 and POLR2A gene consequently led to transcriptional repression of the *POLR2A* gene, resulting in retarded cell proliferation of cancer cells. Furthermore, the impaired nuclear transport of CD26 by treatment with an endocytosis inhibitor or expressions of deletion mutants of CD26 reversed the POLR2A repression induced by YS110 treatment. These findings reveal that the nuclear CD26 functions in the regulation of gene expression and tumor growth, and provide a novel mechanism of mAb-therapy related to inducible translocation of cell-surface target molecule into the nucleus.

Citation: Yamada K, Hayashi M, Madokoro H, Nishida H, Du W, et al. (2013) Nuclear Localization of CD26 Induced by a Humanized Monoclonal Antibody Inhibits Tumor Cell Growth by Modulating of POLR2A Transcription. PLoS ONE 8(4): e62304. doi:10.1371/journal.pone.0062304

Editor: Arun Rishi, Wayne State University, United States of America

Received December 4, 2012; **Accepted** March 19, 2013; **Published** April 29, 2013

Funding: This study was supported by the Program for Promotion of Fundamental Studies in Health Sciences of the National Institute of Biomedical Innovation (07–17 to T.Y. and C.M.), a Grant-in-Aid for Scientific Research (B) (23390086 to T.Y. and 22790355 to M.H.) and Global COE Program "Education and Research Center for Stem Cell Medicine" (to K.Y.) from the Ministry of Education, Culture, Sports, Science and Technology of Japan, and a Grant-in-Aid for Drug Design Biomarker Research (H24-B10-003 to T.Y. and C.M.) from the Ministry of Health, Labor and Welfare. The funders had no role in study design, data collection and analysis, decision to publish, or preparation of the manuscript.

Competing Interests: The authors have declared that no competing interests exist.

* E-mail: taketo@a5.keio.jp

Introduction

CD26 is a type II membrane-spanning glycoprotein that possesses intrinsic dipeptidyl peptidase IV (DPPIV) activity [1], and is implicated in a wide variety of physiological processes, including glucose metabolism, homing and activation of T lymphocytes, and cell adhesion [2,3]. CD26 has also been identified as one of the cell surface markers associated with various types of cancers and a subset of cancer stem cells in malignant mesothelioma and colorectal cancer [4,5,6]. Recent studies have suggested that CD26 expression is involved in tumor growth, tumor invasion, and metastasis [3,7,8]. However, the molecular evidence to support such a role for CD26 in cancer cells has been lacking.

We have previously developed anti-CD26 mAbs that exhibit unambiguous inhibitory effects against the growth of cultured cells and xenografted tumors [9,10]. Notably, the humanized anti-CD26 mAb, YS110, which recognizes the cell membrane-proximal glycosylated region starting at the 20-amino acid flexible stalk region of human CD26, has demonstrated meaningful antitumor effects in malignant mesothelioma models [4]. As it has a human IgG_1 backbone, YS110 can efficiently mediate the recruitment to tumors of human immune effector cells, including natural killer (NK) cells, that express Fc receptors at the cell membrane, in a process of antibody-dependent cellular cytotoxicity (ADCC) [11,12]. This Fc domain-based mechanism is commonly observed with other therapeutic mAbs (e.g., trastuzumab and rituximab) [13,14]. Furthermore, accumulating evidence has shown that these mAbs, which have been approved for cancer therapy, also manifest direct antitumor effects. It has been reported that treatment with trastuzumab, a humanized anti-ErbB2 mAb, reduces the growth of cultured cancer cells by disturbing an associated signaling pathway [11]. In keeping with this, although there is no information on the signaling pathway associated with CD26, YS110 treatment also results in direct inhibitory effects on the proliferation of malignant mesothelioma

cells [4]. However, the molecular mechanism underlying this direct inhibitory effect on cell growth, following YS110 treatment of CD26-positive tumors, has yet to be elucidated.

Most cell surface receptors undergo internalization through certain endocytic process. Endocytosis of these receptors has long been thought to be a negative feedback mechanism for regulating receptor function. However, recent evidence has suggested that internalized receptors are involved in signaling functions of the endosome, or directly transmit signals to the nucleus [15,16]. The latter process is characterized by dynamic nuclear translocation of cargo proteins. Some cell surface receptors, such as epidermal growth factor receptor (EGFR), ErbB2, fibroblast growth factor receptor (FGFR) and CD40, are shown to be translocated into the nucleus, and be consequently involved in transcriptional regulation, cell proliferation, and chemo- and radio-resistance [17,18,19]. This emphasizes the significance of nuclear transport of endocytic cargo in the development of strategies for cell surface receptor-targeted therapy.

Nuclear localization of CD26 has been reported in cultured malignant mesothelioma and malignant T cell lines, and in human thyroid carcinomas [20,21]. However, the functional relevance of nuclear CD26 in cancer cells is far from clear. Our previous studies have shown that the murine anti-CD26 mAb, 1F7, which recognizes the identical epitope to YS110 and has antitumor effects against T cell malignancies, promotes internalization of CD26, and subsequently induces its nuclear accumulation [20,22]. Therefore, we hypothesized that nuclear localization of CD26 is functionally related to the antitumor process following treatment with YS110. In this study, we demonstrated that nuclear translocation of CD26 and YS110 contributed to growth inhibition of malignant mesothelioma cells after YS110 treatment. By performing chromatin immunoprecipitation (ChIP) cloning, we showed that nuclear CD26 interacted with a specific genome target flanking the gene for POLR2A, which is essential for the transcription of many genes [23]. This interaction led to suppression of POLR2A. Furthermore, blocking the nuclear trafficking of CD26 and YS110 prevented both the nuclear translocation of these two proteins and the YS110-induced transcriptional repression of the POLR2A gene. These findings highlight a novel function of CD26 as a transcriptional modulator in the nucleus, and provide insight into the development of cancer therapies through modulation of the nuclear translocation of cell-surface proteins.

Materials and Methods

Cell Culture and Tissue Specimens

The malignant mesothelioma cell lines, JMN, MSTO and MSTO (control, clone 8 and clone 12) [8], the T cell leukemia Jurkat cell line (control and CD26) [22], and the hepatocellular carcinoma Li7 and Kim1 (National Cancer Center Research Institute, Tokyo, Japan) and PLC/PRF/5 (Alex) (American Type culture Collection, Manassas, VA, USA) cell lines were cultured in RPMI 1640 supplemented with 10% fetal bovine serum, 100 units/mL penicillin, and 100 μg/mL streptomycin, under 5% CO_2 at 37°C. Human embryonic kidney 293 cells and the cervical cancer HeLa cell line were cultured in Dulbecco's modified Eagle's medium supplemented with 10% fetal bovine serum, 100 units/mL penicillin, and 100 μg/mL streptomycin, under 5% CO_2 at 37°C. Malignant mesothelioma specimens from autopsies were generously permitted by the bereaved families. This study was approved by the Keio University School of Medicine review board and the permission was obtained (ID number 2012-100-1). The specimens were subjected to immunostaining as described below. The purpose of the study was explained to all patients and their written, informed consent was obtained.

Plasmids, siRNA Transfection, and Reporter Assays

pEGFPC1-Rab5A^{wt}, pEGFPC1-Rab5A^{S34N}, and pEGFPN3-caveolin-1 vectors were a generous gift from Dr. Oikawa (Keio University, Tokyo, Japan). The cDNAs for full-length CD26 (amino acids 1–766), cytoplasmic region-deficient $CD26_{7-766}$ (amino acids 7–766), extracellular region-deleted $CD26_{1-500}$, and $CD26_{1-629}$ were amplified by PCR and introduced into pcDNA3, pFlag-CMV4 (Sigma, St. Louis, MO), and pEGFP-C1 vectors. The PCR primers were: $CD26_{wt}$, 5′-CCG GAA TTC AAT GAA GAC ACC GTGG-3′ and 5′-CGG GAT CCT CAA GGT AAA GAG AAA CA-3′; $CD26_{7-766}$, 5′-CCG GAA TTC AGT TCT TCT GGG ACT GC-3′ and 5′-CGG GAT CCT CAA GGT AAA GAG AAA CA-3′; $CD26_{1-500}$, 5′-CCG GAA TTC AAT GAA GAC ACC GTGG-3′ and 5′-CCG GAA TTC TCA CAA AGC TGA ATTG-3′; and $CD26_{1-629}$, 5′-CCG GAA TTC AAT GAA GAC ACC GTGG-3′ and 5′-CGG GAT CCT CAC CAG CCC CAA ATTG-3′. The resulting vectors were transfected into JMN, HeLa, HEK293, and Li7 cells with Lipofectamine LTX (Invitrogen, Tokyo, Japan). CD26-expressing cells were obtained by selection with G418, as previously described [10].

The sequences of the siRNA (chimeric RNA-DNA) duplexes (RNAi Inc, Tokyo, Japan) were: CHC oligo 1, 5′-CCA AUU CGA AGA CCA AUU UCA-3′ and 5′-AAA UUG GUC UUC GAA UUG GAU-3′; CHC oligo 2, 5′-CUA UGA CAG UCG CGU UGU UGG-3′ and 5′-AAC AAC GCG ACU GUC AUA GUA-3′; caveolin-1, 5′-CCU UCA CUG UGA CGA AAU ACU-3′ and 5′-UAU UUC GUC ACA GUG AAG GUG-3′; POLR2A oligo 1, 5′-CAA CUC CGU ACA AUG CAG ACU-3′ and 5′-UCU GCA UUG UAC GGA GUU GUC-3′; and POLR2A oligo 2, 5′-CAC AUC AAU UGU AUC CGU ACC-3′ and 5′-UAC GGA UAC AAU UGA UGU GAC-3′. Cells were transfected with each siRNA for 48 hours using Oligofectamine reagent (Invitrogen).

For the reporter assays, CAS162 was amplified by PCR and cloned in-frame into pGL3-promoter vector (Promega, Madison, WI). The resulting vector was co-transfected with the phRL-TK vector (Promega). Luciferase assays were performed using a Dual Luciferase Assay Kit (Promega).

Labeling and Preparation of Antibodies

Human IgG_1 and YS110 were labeled using an Alexa647 labeling kit (Invitrogen). Mouse IgG_1 and 1F7 were biotinylated using a biotin labeling kit (Thermo, Rockford, USA).

Cell Surface Biotinylation and Immunoprecipitation

Cells were washed twice with phosphate-buffered saline (PBS) containing 1 mM $CaCl_2$ and 0.5 mM $MgCl_2$ (PBS-CM) at 4°C, and incubated for 12 minutes at 4°C in 1.0 mg/mL of sulfo-N-hydroxysulfosuccinimide (sulfo-NHS)-Biotin (Pierce) dissolved in PBS-CM. To quench unreacted biotin, cells were washed three times with PBS-CM plus 50 mM glycine and twice with PBS-CM [24,25]. After incubation with the indicated antibodies, immunoprecipitation was performed overnight at 4°C, using the CD26 mAb, 1F7 (2 μg), with equal amounts of protein from each fraction. The antibody was bound directly to Protein A Sepharose beads for 1 hour at 4°C. The beads were washed four times with NET-2 buffer (250 mM Tris-HCl pH 7.5, 750 mM NaCl, 0.25% Nonidet P-40) and then subjected to immunoblot analysis [26].

Histology and Immunohistochemistry

Tissues were fixed in 10% neutral buffered formalin, embedded in paraffin, and sectioned at a thickness of 5 μm. Sections were paraffin depleted and rehydrated in a graded series of ethanol solutions. Alternatively, frozen sections were fixed in 4% paraformaldehyde for 20 minutes at room temperature. For histology, sections were stained with hematoxylin and eosin. For immunohistochemistry, sections were washed with PBS, subjected to antigen retrieval by heating at 100°C in 0.01 M sodium citrate (pH 6.0) for 10 minutes, then treated with 3% H_2O_2, before incubation with the following primary antibodies: goat anti-CD26 pAb (AF1180, R&D Systems, Minneapolis, MN) (1:100), rabbit anti-CD26 pAb (H270, Santa Cruz Biotechnology, Inc, Santa Cruz, CA) (1:100), and mouse anti-POLR2A mAb (sc-47701, Santa Cruz) (1:100). Immune complexes were detected by using an ImmPRESS REAGENT KIT (Vector Laboratories, Burlingame, CA) with 3, 3′-diaminobenzidine, and sections were counter-stained with hematoxylin.

Immunoelectron Microscopic Analysis

JMN cells treated with YS110 for 2 hours were fixed in 0.1 M cacodylate buffer (0.1% glutaraldehyde and 4% paraformaldehyde, pH 7.4) on ice overnight. The cells were dehydrated by two 5-minute incubations in 50, 70, 95, and 100% dimethylformamide in water. Cell pellets were incubated in dimethylformamide/lowicryl (1:1) for 30 minutes at room temperature. Sections (8 nm) were sectioned and mounted on copper mesh with 150 grids, incubated with primary antibodies for CD26 (H270, Santa Cruz) and rabbit anti-early endosome marker (EEA)1 pAb (sc-6415, Santa Cruz) overnight, washed four times with PBS, and labeled for 60 minutes with secondary anti-rabbit antibody conjugated with 15 nm immunogold (GE Healthcare, Uppsala, Sweden) or anti-human $F(ab')_2$ or IgG antibodies conjugated with 30 nm immunogold (GAF-352 and GAF-001, EY Laboratories Inc, San Mateo, CA). Sections were washed with 2% uranyl acetate, followed by 4% lead citrate and visualized by electron microscopy.

Immunofluorescence Analysis

Tissues and cultured cells grown on glass coverslides were fixed in 4% paraformaldehyde for 20 minutes at room temperature, then permeabilized with PBS containing 0.2% Triton-X-100 and 1 mg/mL bovine serum albumin (BSA) for 25 minutes. The tissues and cells were washed three times with PBS before incubation at 4°C overnight with the following primary antibodies: goat anti-CD26 pAb (AF1180, R&D Systems) (1:100), rabbit anti-clathrin mAb (610499, BD Pharmingen, San Diego, CA) (1:100), rabbit anti-caveolin-1 pAb (sc-894, Santa Cruz) (1:100), and goat anti-EEA1 pAb (sc-6415, Santa Cruz) (1:200). After washing three times with PBS, the tissues and cells were incubated at room temperature for 30 minutes with the appropriate Alexa Fluor 488-, 594-, or 647-conjugated secondary antibodies and stained with Hoechst 33342 (Invitrogen) for detection of nuclei. Tissues and cells were viewed directly by confocal fluorescence microscopy (FV10i, Olympus, Tokyo, Japan). Quantitation was performed using TissueQuest software (TissueGnostics, Vienna, Austria).

Tracers and Reagents

Alexa Fluor 488-transferrin, Alexa Fluor 488-cholera toxin B, and fluorescein isothiocyanate (FITC)-dextran were purchased from Invitrogen. Nystatin, filipin, monodansylcadaverine (MDC), and chlorpromazine were obtained from Sigma.

Subcellular Fractionation and Immunoblot Analysis

Cells were incubated in medium with/without the CD26 mAbs, 1F7 or 5F8 (2 μg/mL), or control mouse IgG_1 (Dako Cytomation, Glostrup, Denmark). After appropriate incubations, cells were harvested and washed with PBS. Membrane, cytoplasmic and nuclear fractions were extracted using a Qproteome cell compartment kit, according to the manufacturer's instructions (Qiagen, Hilden, Germany), with minor modifications. The membrane fraction contains endosomes and membrane compartment organelles, such as mitochondria and endoplasmic reticulum (ER), as well as cell surface proteins. Alternatively, two cytoplasmic and nuclear fractions were extracted using NE-PER Nuclear and Cytoplasmic Extraction Reagents (Pierce, Thermo Fisher Scientific, Rockford, IL), with minor modifications. The protein concentrations of each fraction were determined using the bicinchoninic acid (BCA) protein assay kit (Pierce Biotechnology). Equal amounts of protein were subjected to 10% sodium dodecyl sulfate (SDS) polyacrylamide gel electrophoresis (PAGE) and transferred to a polyvinylidene fluoride (PVDF) membrane. The membranes were probed with the following antibodies: human CD26 with goat polyclonal antibody (pAb) (AF1180, R&D Systems) (1:200), human POLR2A with mouse mAb (sc-47701, Santa Cruz) (1:200), Na^+/K^+ ATPase as a plasma membrane marker with mouse mAb (sc-21712, Santa Cruz) (1:1000), culreticulin as an ER marker with mouse mAb (612136, BD Pharmingen) (1:2000), calpain-1/2 as a cytoplasmic marker with mouse mAb (Calbiochem, La Jolla, CA) (1:2000), Lamin A/C as a nuclear marker with mouse mAb (sc-7292, Santa Cruz) (1:200), and nucleostemin as a nuclear marker with mouse mAb (Qiagen) (1:1000). Signals were detected by enhanced chemiluminescence (ECL). The relative amounts of CD26 expressed in representative experiments were quantitatively analyzed using ImageQuant 350 software (GE Healthcare), and indicated as the percentage CD26 expression in each fraction.

Chromatin Immunoprecipitation Assay

Chromatin immunoprecipitation was performed using a Simple ChIP Kit (Cell Signaling Technology, Tokyo, Japan), according to the manufacturer's instructions. Cells treated with control human IgG_1 or YS110 were fixed in 1% formaldehyde, and sonicated. After centrifugation, the supernatants containing immunocomplexes were incubated with anti-human IgG_1 or goat anti-CD26 pAb (AF1180, R&D Systems) at 4°C overnight, and then for a further 2 hours with protein G-conjugated magnetic dynabeads. After the immunocomplexes were washed six times with washing buffer, DNA was reverse cross-linked by incubation at 65°C for 2 hours and used for cloning, or as a template for PCR. The identified CAS162 sequence was: 5′-AGC TGA AGT AAA AGG ACT TGG GGG TAA TAC GCT AGT TTT AGC CGG CTA TTT TTC CCC CTT TCA TTA GCA CCT TAA TGT GGT ATC AAT GTT CTA CAT CCT CTG CAA GTC ATT TCT GAT TTA CCT GAG GTA-3′. The PCR primer sequences for CAS162 were: 5′-AGC TGA AGT AAA AGG ACT TGG-3′ and 5′-TAC CTC AGG TAA ATC AGA AAT GAC-3′.

Cloning of DNA Fragments

Immunoprecipitated DNA fragments were cloned into the PCRII Blunt TOPO Vector (Invitrogen). Each DNA sequences were searched using Blast analysis and the National Institutes of Health Entrez Genome Project database.

Electrophoretic Mobility Shift Assay (EMSA)

Double-stranded oligonucleotides containing the 129-bp CD26-associated sequence (CAS) 162 were labeled with biotin using a Biotin 3′ End DNA Labeling Kit (Thermo Fisher Scientific). Nuclear extracts were prepared from JMN cells treated with YS110 (2 μg/mL) for 2 hours, using the NE-PER Nuclear and Cytoplasmic Extraction Reagent Kit (Thermo Fisher Scientific). EMSA was performed using the LightShift Chemiluminescent EMSA Kit (Thermo Fisher Scientific) according to the manufacturer's instructions, with minor modifications. The reaction products were separated by electrophoresis in a 5% non-denaturing polyacrylamide gel (Invitrogen) in 0.5% TB. In competition experiments, nuclear extracts were pre-incubated with a 100-fold excess of intact competitive CAS162 oligonucleotides before biotin-labeled CAS162 was added.

Quantitative RT-PCR Analysis

Total RNA was extracted from cultured cells with RNeasy mini kits (Qiagen) according to the manufacturer's instructions. Reverse transcription of purified RNA was performed using a PrimeScript RT-PCR kit (Takara Bio Inc, Shiga, Japan), according to the manufacturer's instructions. Quantification of all gene transcripts was performed by qPCR, using SYBR Premix Ex Taq II and a Thermal Cycler Dice Real Time System (Takara). The primer pairs were: POLR2A, 5′-GCA TGG CAG AGG AGT TTC GGCT-3′ and 5′-ATT TCC CCG GGA TGC GCA ATGG-3′; and GAPDH, 5′-CCA GCC GAG CCA CAT CGC TC-3′ and 5′-ATG AGC CCC AGC CTT CTC CAT-3′.

Proliferation Assay

Cells were incubated in 96-well plates in media alone or with CD26 mAb (0.02, 0.2, 2, or 20 μg/mL) in a total volume of 100 μL (2.5×10^3 cells/well). After 24 or 48 hours of incubation at 37°C, 2-(2-methoxy-4-nitrophenyl)-3-(4-nitrophenyl)-5-(2,4-disulfophenyl)-2H-tetrazolium (WST) (Nacalai Tesque Inc, Tokyo, Japan) was added to each well. After a further 1 hour of incubation, the water-soluble formazan dye, 1-methoxy-5-methylphenazinium, formed upon bio-reduction in the presence of an electron carrier, was measured in a microplate reader (Bio-Rad) at 450 nm. All samples were assayed in triplicate, and the results reported were means of triplicate wells.

Xenograft Model Using Human Mesothelioma Cell Lines

NOD/Shi-scid, IL-2 receptor gamma null (NOG) mice were obtained from the Central Institute for Experimental Animals. JMN cells (1×10^6) were implanted subcutaneously in the back flank of NOG mice. Mice were injected intratumorally with control human IgG_1 (n = 3) or YS110 (n = 3) at doses of 8 mg/kg body weight. Parental MSTO cells or MSTO cells stably expressing CD26 were inoculated into the thoracic cavities of NOG mice. Thereafter, mice were intraperitoneally injected with control human IgG_1 (n = 3), or YS110 (10 μg per injection) (n = 3), commencing on the day of cancer cell injection. Each antibody was administered three times per week. Mice were then monitored for the development and progression of tumors. Tumor size was determined by caliper measurement of the largest (x) and smallest (y) perpendicular diameters, and was calculated according to the formula $V=\pi/6\times xy^2$.

All experiments were approved by the Animal Care and Use Committee of Keio University and were performed in accordance with the institute guidelines.

Statistical Analysis

Data are presented as means ± SD and were assessed for statistical significance using the unpaired Student's t test.

Results

Anti-CD26 Monoclonal Antibodies are Translocated to the Nucleus in CD26-Positive Cancer Cells

The cellular localization of YS110 in malignant mesothelioma cells was examined to elucidate the role of humanized mAb YS110 in its antitumor effect on cancer cells. The CD26-positive malignant mesothelioma cell line, JMN (the proliferation of which was reduced after YS110 treatment) (Fig. S1A), was chosen, and the cells were treated with YS110 labeled with Alexa647 dye (Alexa-YS110). After treatment, Alexa-YS110 was internalized and diffused throughout the cytoplasm within 30 min (Fig. 1A). Furthermore, at 30 min to 2 h, Alexa-YS110 localized within the nucleus in the form of dots, as well as in the cytoplasm (Fig. 1A). This observation of several dots of Alexa-YS110 that colocalized with a nuclear marker (Hoechst 33342) in a single cell defined the cells containing YS110 in the nucleus. Over 4 h after treatment with Alexa-YS110, the number of cells retaining Alexa-YS110 in the nucleus was apparently decreased (Fig. 1A). To exclude the possibility that this nuclear localization of Alexa647 fluorescence was due to free Alexa647 fluorescent probe that had detached from YS110, indirect immunostaining analysis was performed with anti-human IgG. Nuclear staining of YS110 was apparent in JMN cells treated with unlabeled YS110 prior to fixation (Fig. 1B). Furthermore, on closer examination of YS110 nuclear localization using TissueQuest software [27], it was estimated that about 70% of the nuclear YS110 resided away from the nuclear membrane (NM), with the remaining YS110 distributed diffusely along the perimeter of the inner NM (Fig. 1C). These results suggested that YS110 appears to localize in the nucleus.

To confirm the nuclear localization of this antibody, biochemical analysis was performed using a T cell leukemia cell line (Jurkat) that is negative for CD26, and a Jurkat cell line that was stably transfected with CD26 expression vector (Jurkat/CD26). These cells were treated with biotin-conjugated control IgG_1 (biotin-IgG_1), or with biotin-conjugated murine anti-CD26 mAb, 1F7 (biotin-1F7), which recognizes an epitope identical to that recognized by YS110 and has an antitumor effect on T cell malignancies (Fig. S1B) [10]. Upon treatment with biotin-1F7, two biotin bands comparable in size to the heavy and light chains of 1F7 were detected in the nuclear fraction of Jurkat/CD26 cells, whereas no bands were detected in any fraction from control Jurkat/mock cells (Fig. 1D), indicating that 1F7 was localized in the nuclear fraction of CD26-positive Jurkat cells. Furthermore, a pull-down assay with streptavidin demonstrated the association of biotin-1F7 with CD26 in the nuclear fraction of biotin-1F7-treated Jurkat/CD26 cells, but not in cells treated with biotin-IgG_1 (Fig. 1D, lower panels). Similarly, co-localization of CD26 and YS110 was also observed by immunoelectron microscopic analysis using different sized immunogold particles (15 nm for CD26, 30 nm for YS110) (Fig. 1E). Taken together, these results suggested that two anti-CD26 mAbs (YS110 and 1F7) with antitumor effects on cancer cells are transported to the nucleus in a CD26-dependent manner.

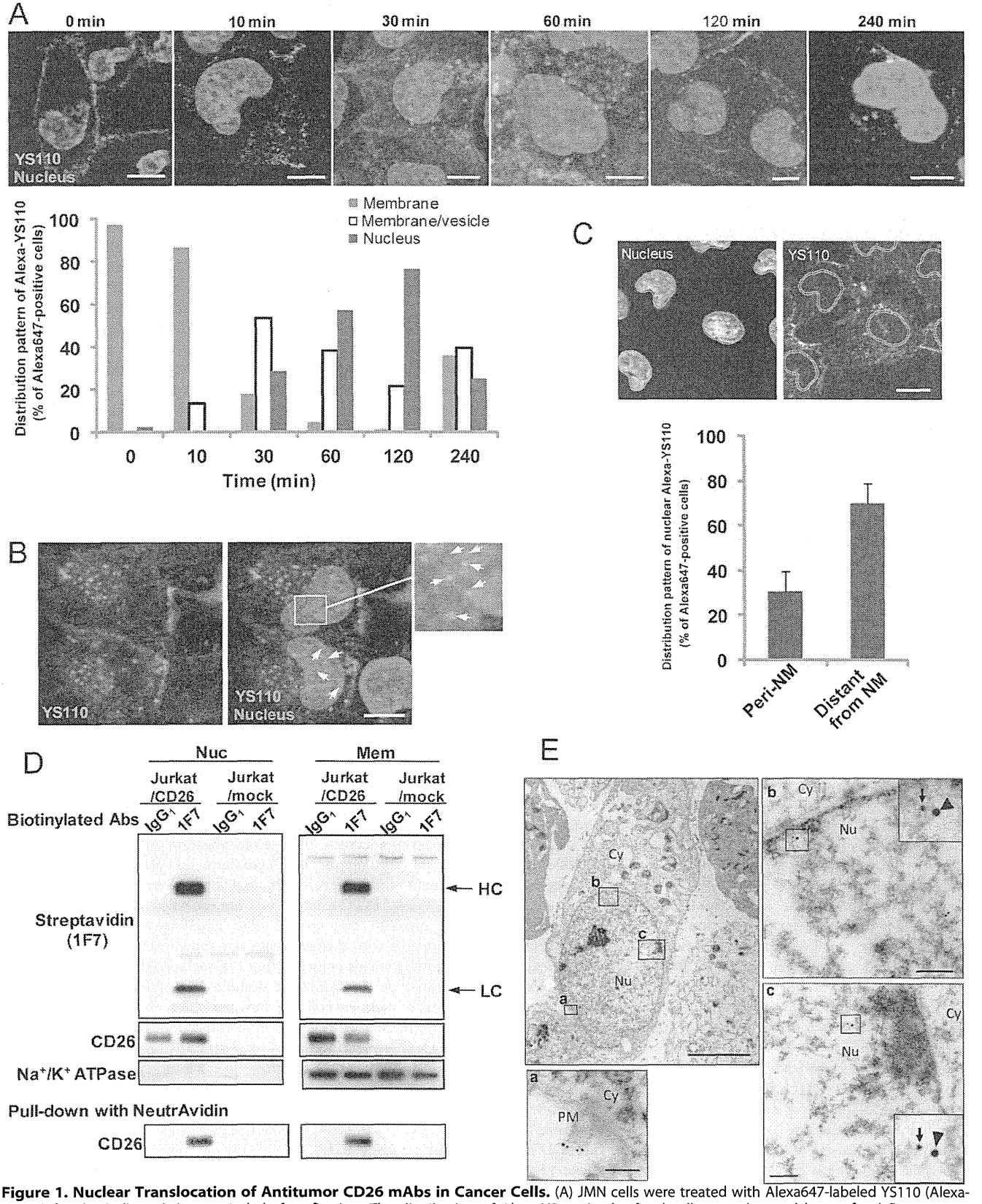

Figure 1. Nuclear Translocation of Antitumor CD26 mAbs in Cancer Cells. (A) JMN cells were treated with Alexa647-labeled YS110 (Alexa-YS110) for the indicated time periods before fixation. The distribution of Alexa-YS110 in the fixed cells was observed by confocal fluorescence microscopy (upper panels). To quantitate these observations, fixed JMN cells retaining Alexa-YS110 were categorized into three types [28]: the cell containing YS110 predominantly observed on the cell surface (red bar); the cell containing Alexa-YS110 present on both the cell surface and in cytosolic vesicles (white bar); the cell containing Alexa-YS110 observed in the nucleus (blue bar). The categorization was performed by confocal

fluorescence microscopy of more than 50 cells for each incubation time (lower panel). Scale bars, 10 μm. (B) Immunofluorescence staining with antibody to human IgG_1 in fixed JMN cells, following YS110 treatment for 1 hour, and staining with Hoechst 33342. Localization of YS110 (green) in the nucleus (red) appears as yellow, as indicated by arrows. Scale bars, 10 μm. (C) Identification of the nuclear membrane (NM) was performed using TissueQuest software. The distribution of Alexa-YS110 in the nucleus was subdivided into two categories: close to (within 1 μm; peri-NM) or distant from NM, in JMN cells treated with Alexa-YS110 for 2 hours. Data are means ± SD for more than 20 cells. Scale bar, 10 μm. (D) Jurkat/mock or Jurkat/CD26 cells were incubated with biotin-labeled control IgG_1 or 1F7 for 1 hour. Nuclear (Nuc) and membrane (Mem) extracts of these cells were pulled-down with Neutravidin, and then subjected to immunoblot analysis using streptavidin or antibodies to CD26 or Na^+/K^+ ATPase (membrane marker). HC, heavy chain; LC, light chain. (E) Immunogold labeling for CD26 and YS110 on ultrathin sections demonstrated the localization of these proteins in JMN cells. The arrow and arrowhead indicate CD26 (15 nm) and YS110 (30 nm) in the plasma membrane (a) and the nucleus (b and C), respectively. Scale bars, 5 μm and 200 nm (a, b and c). PM, plasma membrane; Cy, cytoplasm; Nu, nucleus.
doi:10.1371/journal.pone.0062304.g001

YS110 Induces Nuclear Localization of CD26, and Deletion of the Extracellular Region of CD26 Prevents the Nuclear Transport of CD26 and YS110

To investigate the nuclear localization of CD26 in cancer cells, four malignant mesothelioma cell lines that differed in CD26 expression status were first examined: one that expressed CD26 endogenously (JMN); one CD26-negative cell line (MSTO); and two cell lines that expressed CD26 exogenously (MSTO/clone8, MSTO/clone12). Under normal culture conditions, the single full-length form of CD26 was detected, not only in the membrane and cytoplasmic fractions, but also in the nuclear fraction of JMN [20], MSTO/clone8 and MSTO/clone12 (MSTO/CD26) cells (Fig. 2A). Similar result was obtained in primary tumor of two malignant mesothelioma patients (Fig. 2A). Furthermore, nuclear localization of CD26 in JMN cells was confirmed by immunoelectron microscopy (Fig. 2B). These results suggested that full-length CD26 is translocated to the nucleus, as previously reported [20].

We next investigated the potential effect of YS110 on nuclear localization of CD26 in cancer cells. Western blot analysis of JMN cells showed that the amount of CD26 in the nuclear fraction of the cells was markedly increased by YS110 treatment, peaking at 2 h and then decreasing by 4 h to close to the original level (Fig. 2C). Similar results were obtained after 1F7 treatment of Jurkat/CD26 cells (Fig. S2A), and after YS110 treatment of Li7 hepatocellular carcinoma cells that expressed CD26 exogenously (Fig. S2B), suggesting that YS110 and 1F7 induced nuclear translocation of CD26 in cancer cells.

To evaluate the relevance of the nuclear localization of CD26 to the nuclear trafficking of YS110, various CD26 deletion mutants were generated to specify the domain of CD26 that was essential for its nuclear localization (Fig. 2D). When transfected into human embryonic kidney (HEK) 293 cells that are negative for CD26, the wild-type ($CD26_{wt}$) and cytoplasmic region-deficient ($CD26_{7-763}$) forms were clearly detected in the nuclear fraction of these cells (Fig. 2D). In contrast, the two partial C-terminal extracellular region-depleted forms ($CD26_{1-500}$ and $CD26_{1-629}$) were not detected in the nuclear fraction, although their cell-surface expression and capacity to bind to YS110 were confirmed (Fig. 2D; Fig. S3A). Similar results were obtained in Li7 cells transfected with $CD26_{wt}$ or $CD26_{1-629}$ constructs (Fig. S2B), indicating that the extracellular domain of CD26 is required for its nuclear transport.

Next, the nuclear trafficking of each CD26 construct and YS110 was examined after YS110 treatment of $CD26_{wt}$ or $CD26_{1-629}$-expressing JMN or HeLa cells, which express higher levels of caveolin-1 than HEK 293 cells [28]. After YS110 treatment of these two GFP-fused $CD26_{wt}$-expressing cell lines, GFP-$CD26_{wt}$ was visible in the nucleus, where it overlapped with Alexa-YS110 fluorescence (Fig. 2E; Fig. S3B). In contrast, no nuclear localization of GFP-$CD26_{1-629}$ and Alexa-YS110 was observed when these cells were transfected with GFP-$CD26_{1-629}$ (Fig. 2E; Fig. S3B). These results suggest that the nuclear trafficking machinery for CD26 mediates the nuclear entry of YS110.

As the nuclear translocation of YS110 and 1F7 appears to rely on the cell-surface expression of CD26 (Fig. 1D), the involvement of cell-surface CD26 in augmented nuclear localization of CD26 by these antibodies was investigated. A cell-surface biotinylation assay using Jurkat/CD26 cells showed that, relative to control, the amount of biotin-labeled CD26 in the nuclear fraction was significantly increased following 1F7 treatment, over the same time course as that of the total CD26 content of the cells after 1F7 treatment (Fig. S2A; S4A), indicating that 1F7 promoted nuclear translocation of cell-surface CD26. Conversely, this phenotype was not seen in cell-surface biotinylated cells treated with another murine anti-CD26 mAb, 5F8, which recognizes a different epitope of CD26 from that recognized by YS110 and 1F7, and which has no antitumor effect on cell growth (Fig. S4B) [22]. These data suggest that antitumor mAbs (YS110 and 1F7) bind to cell-surface CD26, and thereafter are translocated to the nucleus.

Caveolin-Dependent Endocytosis Affects both Endocytosis and Nuclear Translocation of CD26 and YS110

To further characterize the nuclear transport of CD26 and YS110, the involvement of endocytosis in the nuclear translocation of CD26 and YS110 was examined. The process of internalization of cell-surface proteins has been divided into three major mechanisms: clathrin-mediated endocytosis, caveolin-dependent endocytosis, and macropinocytosis [29]. Therefore, we investigated which pathway is used by YS110 to enter the cytosol after binding to cell-surface CD26. To this end, three different endocytotic tracers were employed: Alexa488-labeled transferrin (Alexa-Tf) for the clathrin pathway, Alexa488-labeled cholera toxin B (Alexa-CtxB) for the caveolin pathway, and FITC-dextran for macropinocytosis [30]. Colocalization of Alexa-YS110 was observed throughout the cytoplasm of JMN cells after co-treatment with Alexa-CtxB, but not Alexa-Tf (Fig. 3A; Fig. S5A). While, FITC-dextran was not observed on JMN cells at any time, possibly due to the low reactivity of the cell-surface components with dextran (data not shown). Furthermore, consistent with previous evidence that cell-surface CD26 associates with caveolin-1 at the lipid/raft domain [31], YS110 was found to colocalize with caveolin-1, but not with clathrin heavy chain (CHC), which is a key component of the clathrin pathway (Fig. 3B, 3C). These observations suggest that YS110 may utilize caveolin-dependent endocytosis to enter the nucleus.

In turn, the significance of the caveolin-dependent pathway for the nuclear translocation of CD26 and YS110 was investigated. When JMN cells were depleted of caveolin-1 by transfection with small interfering RNA (siRNA) for caveolin-1 mRNA, significant reductions in both endocytosis and nuclear localization of YS110 were observed in JMN cells treated with Alexa-YS110 (Fig. 3C). However, there was no significant difference in the distribution of YS110 between cells treated with control siRNA or siRNA for CHC (Fig. 3B, arrows). Accordingly, disruption of caveolae formation with nystatin, an inhibitor of the caveolin pathway that

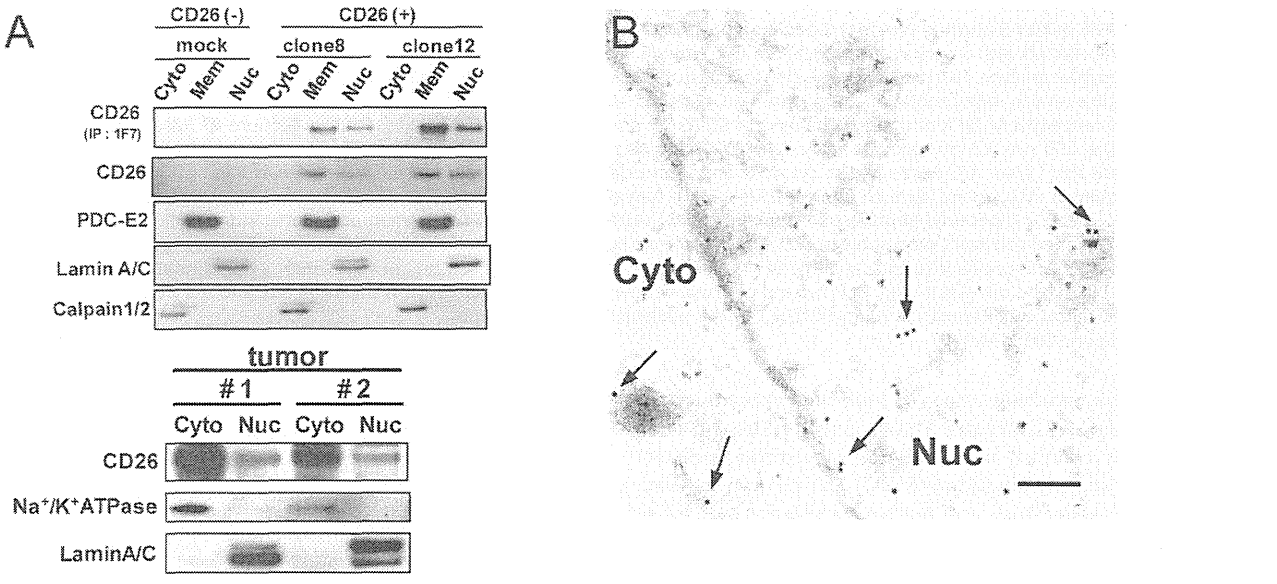
A
CD26 (-)
CD26 (+)
mock
clone8
clone12
Cyto
Mem
Nuc
CD26 (IP : 1F7)
CD26
PDC-E2
Lamin A/C
Calpain1/2
tumor
#1
#2
Cyto Nuc Cyto Nuc
CD26
Na+/K+ATPase
LaminA/C
B
Cyto
Nuc
C
Cyto
Nuc
2 h
4 h
med
IgG1
YS110
CD26
Na+/K+ATPase
LaminA/C
D
TM
GD
DPPIV
1 7 29 85 321 627 740 766
CD26wt 1 766
CD26 7-766 7 766
CD26 1-500 1 500
CD26 1-629 1 629
Flag
Flag-CD26W1
Flag-CD26 7-766
Flag-CD26 1-500
Flag-CD26 1-629
Cyto
Mem
Nuc
Flag
Nucleostemin
E
YS110 (-)
YS110 (+)
GFP
YS110
Nucleus
merge
GFP-CD26wt
GFP-CD26 1-629

Figure 2. Anti-CD26 mAbs Enhance Nuclear Localization of CD26. (A) Nuclear (Nuc), cytoplasmic (Cyto), and membrane (Mem) fractions of MSTO cells stably transfected with empty vector (mock) or CD26 (clone8 and clone12) were prepared (Qiagen kit), immunoprecipitated with 1F7, and subjected to immunoblot analysis. Nuclear (Nuc) and cytosolic (Cyto) fractions of tumors from two malignant mesothelioma patients were prepared (Thermo kit), and subjected to immunoblot analysis. Lamin A/C, Calpain 1/2, and PDC-E2 and Na^+/K^+ ATPase were used as nuclear, cytoplasmic and membrane markers, respectively. (B) Immunogold staining of CD26 (15 nm gold particles, arrows) in ultrathin sections of JMN cells. Cyto, cytoplasm; Nu, nucleus. Scale bar, 200 nm. (C) Immunoblot analysis of CD26 in nuclear and cytosolic fractions of JMN cells treated with YS110 for the indicated times. Na^+/K^+ ATPase and Lamin A/C were used as cytosolic and the nuclear markers, respectively. (D) Diagram of each CD26 deletion mutant (left picture). CD26 contains a cytoplasmic domain (amino acids 1–6), a transmembrane domain (TM) (amino acids 7–29), a glycosylated domain (GD) (amino acids 85–321), and a dipeptidyl peptidase IV domain (DPPIV) (amino acids 627–740). Human embryonic kidney (HEK) 293 cells transiently expressing each flag-tagged construct were subjected to subcellular fractionation and immunoblot analysis with antibodies to Flag and nucleostemin (as a nuclear marker). (E) Immunofluorescence analysis of HeLa cells transfected with GFP-$CD26_{wt}$ or GFP-$CD26_{1-629}$ and treated or not treated with Alexa-YS110 for 1 hour. In the merged image, GFP-fused proteins are shown in green, Alexa-YS110 is shown in red, and the nucleus is shown in blue. Arrows indicate colocalization of Alexa-YS110 and $CD26_{wt}$ in the nucleus. Scale bars, 10 μm.
doi:10.1371/journal.pone.0062304.g002

binds to cholesterol, markedly impaired both the endocytosis and nuclear localization of CD26 and YS110 in YS110-treated cells (Fig. 3D, 3E). In contrast, two inhibitors of clathrin-mediated endocytosis, monodansylcadaverine (MDC) and chlorpromazine, did not affect the endocytosis and nuclear localization of YS110 (Fig. 3D; Fig. S5B). These results indicated that caveolin-dependent endocytosis is required for the nuclear translocation of CD26 and YS110.

Endocytic transport is regularly exerted by Rab small G proteins [32,33]. Rab5A organizes a membrane domain that defines the site of entry into early endosomes through its effector proteins, including early endosome antigen (EEA)1. Previous studies have indicated that EEA1 associates with EGFR and ErbB2 in the nucleus [34,35]. Therefore, we examined whether the nuclear trafficking of YS110 involved an early endocytic pathway. Immunostaining with EEA1 antibody showed that Alexa-YS110 colocalized with EEA1 in the nucleus within 30 min (Fig. S5C, lower panels). YS110-EEA1 complex in the nucleus was also observed by electron microscopy with the respective immunogold particle-conjugated antibodies (15 nm for EEA1, 30 nm for YS110) (Fig. S5D). Importantly, expression of the dominant-negative form of Rab5A ($Rab5A^{S34N}$) suppressed nuclear translocation of Alexa-YS110 (Fig. S5E). These data therefore strongly support the significance of endocytic trafficking in the nuclear translocation of YS110.

Nuclear Localization of CD26 and YS110 in a Xenograft Model for Malignant Mesothelioma

To evaluate whether CD26 and YS110 are translocated to the nucleus *in vivo*, a xenograft model was established using NOD/Shi-scid, IL-2 receptor gamma null (NOG) mice that constitutively lack T, B, and NK cell activities, and were subcutaneously inoculated with JMN cells. The tumors were allowed to develop in the xenografted mice for about two months after inoculation, and exhibited sarcomatoid malignant mesothelioma-like histology (Fig. 4A, 4F). In a similar model, we confirmed that administration of YS110 apparently reduced the tumorigenicity of JMN [4] and MSTO/clone12 (MSTO/CD26) cells (Fig. S6). Direct intra-tumoral injection of Alexa-YS110 into the center of the JMN tumors resulted in the nuclear accumulation of Alexa-YS110, as observed in tumor sections from the mice 1 h (Fig. S7) and 6 h (Fig. 4H, 4I, 4J) after Alexa-YS110 injection. Conversely, there was no Alexa647-fluorescence at any tumor sites injected with Alexa-control IgG_1 (Fig. 4C, 4D, 4E; Fig. S7). Furthermore, CD26 also localized as vesicle-like structures in the cytosol and nucleus after Alexa-YS110 administration (Fig. 4G, 4I), whereas it was located at the cell surface and in the cytoplasm in tumors treated with Alexa-IgG_1 (Fig. 4B, 4D). From these results, we conclude that CD26 and YS110 are translocated to the nucleus of CD26-positive cancer cells as a result of treatment with YS110.

Nuclear CD26 Associates with Target Genomes and Represses POLR2A Gene Expression

To address the potential role of nuclear CD26 in response to YS110 treatment, chromatin immunoprecipitation (ChIP) cloning was performed to explore the possibility that nuclear CD26 associates with genomic targets as a transcriptional regulator. Putative associated DNA fragments were collected from lysates of JMN cells stimulated with YS110 for 3 h, and then identified as candidate sequences, with the loci within 3.0 kilobase pairs (kbp) of genes and introns being identified as nuclear CD26-associated sequences (CAS) (Fig. 5A). Among these, we focused on the CAS162 sequence, which is located 894 bp downstream of the gene that encodes polymerase (RNA) II (DNA directed) polypeptide A (POLR2A; NM_000937) (Fig. 5B). POLR2A is the largest subunit of RNA polymerase II, which is essential for the transcription of most protein-coding genes [23]. Therefore, further investigation was carried out on the relationship between CAS162 and CD26. ChIP analysis using primers flanking CAS162 revealed that the interaction between CD26 and CAS162 was dramatically increased in JMN cells treated with YS110, as compared to those treated with control IgG_1 (Fig. 5C; Fig. S8A). The small amount of PCR product in control goat IgG-immunoprecipitant from the YS110-treated cells was likely due to the binding of YS110 to protein G sepharose on the dynabeads (Fig. 5C). The association between CD26 and the CAS162 sequence was confirmed by electrophoretic mobility shift assay (EMSA). A shifted complex with biotinylated 129 bp CAS162 was apparently enhanced when recombinant CD26 was added to nuclear extracts of JMN cells (Fig. 5D, arrow). On the other hand, additional YS110 did not affect any shifts or the amount of biotinylated-CAS162 (Fig. 5E, arrow), indicating that CD26 plays a key role in the assembly of the CD26/YS110/CAS162 complex.

To evaluate the transactivation potential of CAS162 in cancer cells, luciferase assays were performed in several cancer cell lines. In contrast to transfection with control vector, transfection with CAS162 reporter significantly increased luciferase activity in several cancer cell lines: two malignant mesothelioma lines (MSTO, JMN); and two hepatocellular carcinoma cell lines (Li7, Kim1) (Fig. 5F, 5G; Fig. S8B), suggesting that CAS162 may contain the regulatory element for POLR2A gene expression. Furthermore, we investigated whether nuclear localization of CD26 would affect this CAS162-regulating luciferase activity. The luciferase activity was significantly reduced in CAS162 reporter-expressing MSTO/CD26 cells, in which CD26 is physiologically localized to the nucleus, compared with CAS162 reporter-expressing, CD26-negative MSTO cells (Fig. 2A, 5F). Furthermore, in CAS162 reporter-expressing, CD26-positive JMN cells, YS110 treatment induced a significant decrease in the relative luciferase activity (Fig. 5G). These data suggest that the CD26-

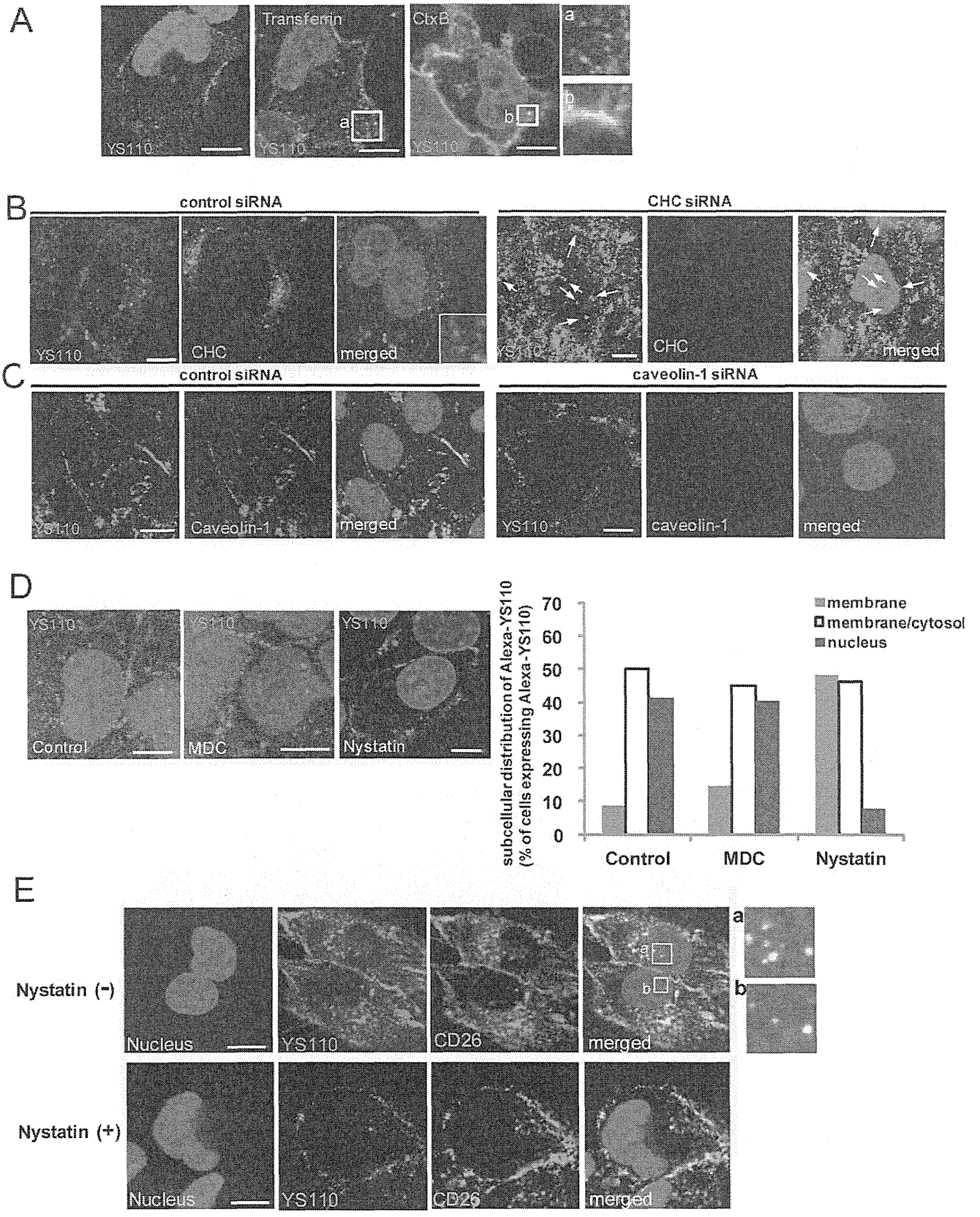

Figure 3. Caveolin-Dependent Endocytosis Mediates the Nuclear Translocation of CD26 and YS110. (A) JMN cells were incubated with Alexa-YS110 and PBS, Alexa488-Transferrin (Alexa-Tf), or Alexa488-Cholera toxin B (Alexa-CtxB) for 5 minutes In the merged images, YS110 is shown in red, the tracers are shown in green, and the nucleus is shown in blue. Colocalization of YS110 and the respective tracer appears as yellow. The boxed

region in the panels shows localization of Alexa-YS110 and Alexa-Tf (a) or Alexa-CtxB (b) at high magnification. Scale bars, 10 μm. (B) JMN cells were treated with siRNA for non-silencing (NS) or siRNA for clathrin heavy chain (CHC). Images show immunofluorescence staining for YS110 (red), clathrin heavy chain (CHC, green) and Hoechst 33342 (blue) in fixed JMN cells, following Alexa-YS110 treatment for 30 minutes. Scale bars, 10 μm. (C) JMN cells were treated with siRNA for NS or siRNA for caveolin-1. Images show immunofluorescence staining for YS110 (red), caveolin-1 (green) and Hoechst 33342 (blue) in fixed JMN cells, following Alexa-YS110 treatment for 30 minutes. Scale bars, 10 μm. (D) JMN cells were pre-treated with dimethyl sulfoxide (DMSO), monodansylcadaverin (MDC) (250 μM), or nystatin (50 μg/mL) for 30 minutes, and then stimulated with Alexa-YS110 for 30 minutes. Quantification of the number of cells in which Alexa-YS110 was localized on the cell surface (membrane), in the cytosol (membrane/cytosol), and in the nucleus (nucleus), was performed by confocal fluorescence microscopy of more than 50 cells for each incubation time (right panel). Scale bars, 10 μm. (E) JMN cells were pretreated with or without nystatin prior to incubation with Alexa-YS110 for 30 minutes. In the merged images, YS110 is shown in red, CD26 is shown in green, and the nucleus is shown in blue. Colocalization of YS110 and CD26 in the nucleus appears as white in the boxed region (a and b). Scale bars, 10 μm.
doi:10.1371/journal.pone.0062304.g003

CAS162 interaction negatively regulates POLR2A gene expression.

Nuclear Translocation of CD26 Induced by Treatment with YS110 and 1F7 Suppresses POLR2A Expression in Cultured Cancer Cells and a Xenograft Model for Malignant Mesothelioma

To investigate whether the nuclear translocation of CD26 suppresses POLR2A expression, we first evaluated POLR2A expression in cancer cells after YS110 treatment, as YS110 induced the nuclear localization of CD26 (Fig. 2C). Quantitative reverse transcription polymerase chain reaction (qRT-PCR) analysis for POLR2A mRNA showed a significant reduction in POLR2A expression in JMN cells after treatment with YS110 or 1F7, compared with controls (Fig. 6A, 6B; Fig. S9A). Concomitantly, Western blot analysis also revealed that YS110 treatment decreased the levels of POLR2A protein in the cells (Fig. 6C). Similar results were observed in MSTO/CD26 cells treated with YS110 (Fig. S9B). Furthermore, reduced expression of POLR2A was observed in the JMN xenograft model after YS110 administration (Fig. 6D, 6E). Thus, antitumor CD26 mAbs (YS110 and 1F7) appeared to induce suppression of POLR2A expression at both the mRNA and protein levels.

To further explore the relevance of nuclear transport of CD26 and YS110 to altered expression of POLR2A mRNA, JMN cells were challenged with nystatin prior to YS110 treatment. qRT-PCR analysis showed that YS110-induced transcriptional repression of POLR2A was significantly over-ridden by nystatin treatment (Fig. 6F). Furthermore, given that the $CD26_{1-629}$ mutant did not enter the nucleus, Li7 cells were transfected with control vector, $CD26_{wt}$, or $CD26_{1-629}$, and expression of POLR2A mRNA after IgG_1 or YS110 treatment was compared by qRT-PCR. In $CD26_{wt}$-expressing Li7 cells, POLR2A expression was significantly decreased after YS110 treatment, compared with control (Fig. 6G). Conversely, $CD26_{1-629}$-expressing cells exhibited apparent resistance to YS110 treatment (Fig. 6G). Taken together, these results strongly suggested that nuclear localization of CD26 induced by YS110 treatment leads to suppression of POLR2A expression.

To exclude Fc domain-dependency of this reduced POLR2A expression, YS110 lacking the Fc region was prepared by pepsinization. Pepsin digestion of YS110 leads to truncation of the Fc region to yield the $F(ab')_2$ form of YS110 (Fig. S10). Treatment with the $F(ab')_2$ form of YS110 markedly decreased the levels of POLR2A transcript in JMN cells, which was similar to the result obtained with the original form of YS110 (Fig. 6A). This indicated that the effect of YS110 on transcriptional repression of POLR2A is independent of the Fc domain of YS110.

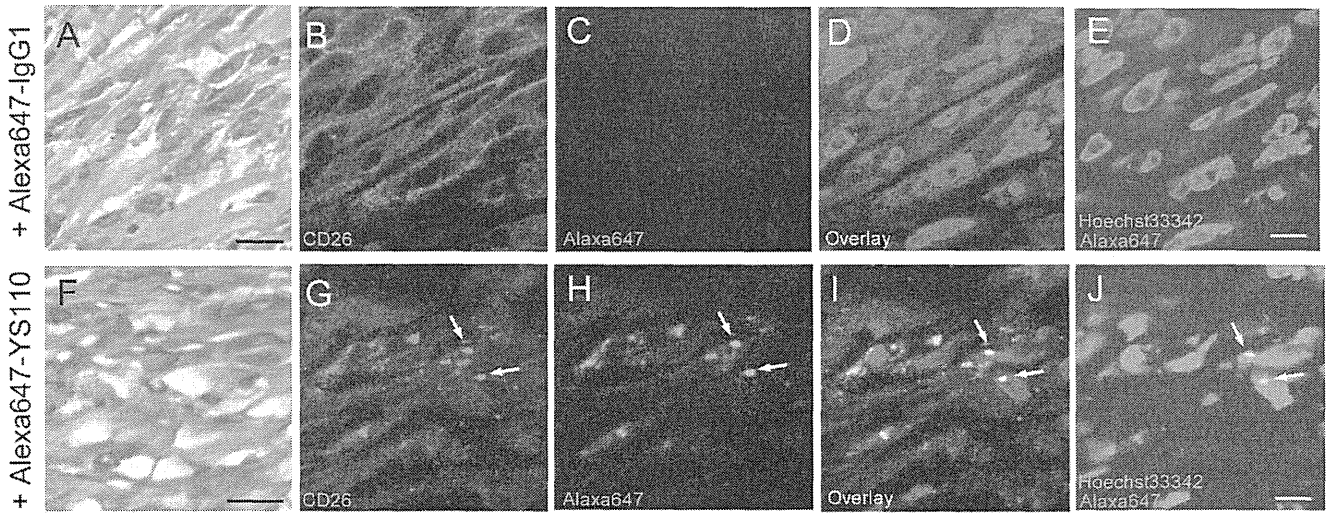

Figure 4. YS110 and CD26 Translocate to the Nucleus *In Vivo*. H&E staining (A and F) and fluorescence analysis (B–E and G–J) of malignant mesothelioma tumors in NOG mice inoculated with JMN cells were shown. These tumors were removed 6 hours after one intratumoral injection (1 μg/a tumor, volume is 100 μL) of Alexa647-human IgG_1 (A–E) or Alexa647-YS110 (F–J). In the overlaid image, CD26 expression is indicated in red (B, D, G, and I), Alexa647-labeled antibodies are shown in green (C, D, H and I), and the nucleus is shown in blue (D and I). Colocalization of CD26 and YS110 in the nucleus appears as white (I, arrows). This localization of Alexa647-labeled antibody (green) in the nucleus (red) is confirmed as yellow (arrows) (J). Similar results were obtained with three different mice. Scale bars, 20 μm (A and F) and 10 μm (B–E and G–J).
doi:10.1371/journal.pone.0062304.g004

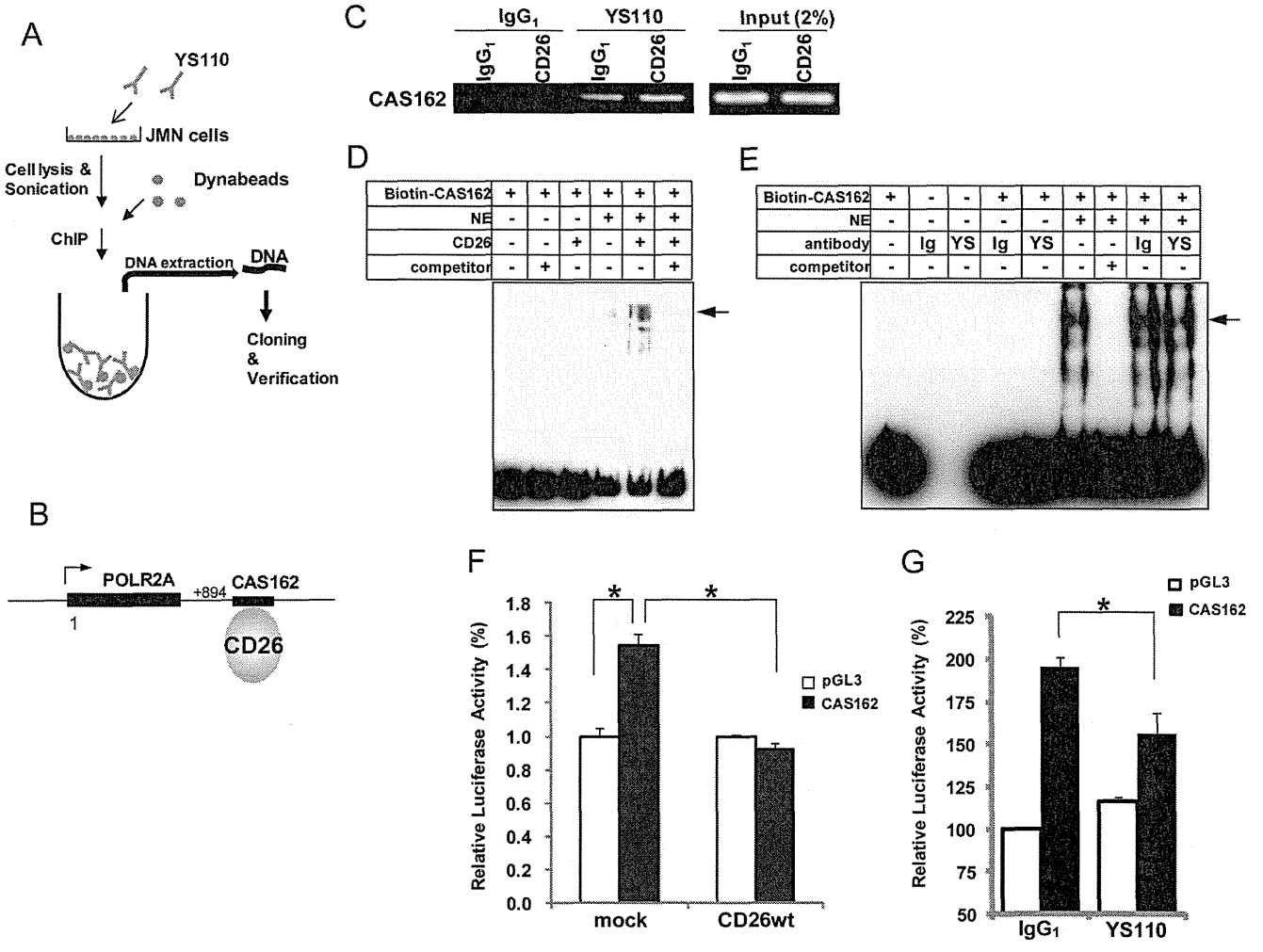

Figure 5. Nuclear CD26 Associates with a POLR2A-Related Genome Sequence Following YS110 Treatment. (A) Schematic diagram of chromatin immunoprecipitation (ChIP) cloning. JMN cells pretreated with YS110 for 3 hours were fixed, sonicated, and immunoprecipitated with Dynabeads to collect YS110-CD26-DNA complexes. The DNA fragments were cloned and identified by sequencing. The identity of candidate sequences was confirmed using data from GeneBank. (B) Genomic location of the CAS162 sequence. The 129-bp CAS162 sequence is located 894 bp downstream from the POLR2A gene. (C) ChIP analysis of CAS162 in JMN cells treated with control human IgG_1 or YS110 for 3 hours. Similar results were obtained in three independent experiments. (D) Biotin-labeled CAS162 oligonucleotide was used for electrophoretic mobility shift assay (EMSA). Nuclear extract (NE) was also collected from JMN cells pretreated with YS110 for 3 hours. After 20 minutes at room temperature the extracts, with or without recombinant CD26, were subjected to immunoblot analysis with streptavidin. Non-biotinylated CAS162 was used as a competitor. Arrow indicates the CD26-CAS162 oligonucleotide complex. (E) Biotin-labeled CAS162 oligonucleotide was used for EMSA. NE was collected from JMN cells. After 20 minutes at room temperature the extracts, with or without antibodies, were subjected to immunoblot analysis with streptavidin. Arrow indicates the CD26-CAS162 oligonucleotide complex. YS, YS110; Ig, IgG_1. (F) MSTO (mock or $CD26_{wt}$) cells were co-transfected with empty vector (pGL3) or CAS162 and phRL-TK, and relative luciferase activity was measured using a luminometer. Data were normalized for luciferase activity in cells transfected with phRL-TK, and are presented as mean values (± SD) from three independent experiments. *$P<0.025$. (G) JMN cells co-transfected with pGL3 or CAS162 and phRL-TK vector were incubated with control IgG_1 or YS110, and relative luciferase activity was measured using a luminometer. Data were normalized for luciferase activity in JMN cells transfected with phRL-TK, and are presented as mean values (± SD) from three independent experiments. *$P<0.025$.
doi:10.1371/journal.pone.0062304.g005

POLR2A Localizes to the Nucleus, and POLR2A Ablation Suppresses Cell Growth of Cultured Malignant Mesothelioma Cells

POLR2A has been shown to be recruited to the nucleus [23]. Therefore, we examined the pattern of expression of POLR2A in tumor sections from patients with malignant mesothelioma (Fig. 7A), and in JMN (Fig. 6D) and MSTO/CD26 (Fig. 7B) cells, by immunohistochemical analysis. As previously reported for various types of tissues and tumors [36], most of the POLR2A staining was located in the nucleus in these tumors (Fig. 6D, 7A, 7B). Therefore POLR2A appears to be functional in malignant mesothelioma cells.

To examine the functional role of POLR2A in the growth of cancer cells, two RNAi constructs (oligo 1 and oligo 2) were developed to silence POLR2A expression. Both constructs effectively knocked down endogenous POLR2A in JMN cells (Fig. 7C), and obviously inhibited the proliferation of JMN cells (Fig. 7D). This result suggests that POLR2A contributes to the regulation of malignant mesothelioma cell growth.